UNIVERSIDADE ESTADUAL DE CAMPINAS

INSTITUTO DE QUÍMICA

MARCIO CRISTIANO MONTEIRO

STUDY OF THE PROPERTIES OF PRUSSIAN BLUE OBTAINED VIA $[Fe(CN)_5(mpz)]^{2-}$ COMPLEX

ESTUDO DAS PROPRIEDADES DO AZUL DA PRÚSSIA OBTIDO ATRAVÉS DO COMPLEXO $[Fe(CN)_5(mpz)]^{2-}$

CAMPINAS
2016

MARCIO CRISTIANO MONTEIRO

STUDY OF THE PROPERTIES OF PRUSSIAN BLUE OBTAINED VIA $[Fe(CN)_5(mpz)]^{2-}$ COMPLEX

ESTUDO DAS PROPRIEDADES DO AZUL DA PRÚSSIA OBTIDO ATRAVÉS DO COMPLEXO $[Fe(CN)_5(mpz)]^{2-}$

Dissertação de Mestrado apresentada ao Instituto de Química da Universidade Estadual de Campinas como parte dos requisitos exigidos para a obtenção do título de Mestre em Química na área de Química Inorgânica.

Master's thesis presented to the Institute of Chemistry of the University of Campinas as part of the requirements to obtain the title Master's in Chemistry in the area of Inorganic Chemistry.

Supervisor: Prof. Dr. Juliano Alves Bonacin

ESTE EXEMPLAR CORRESPONDE À VERSÃO FINAL DA DISSERTAÇÃO DEFENDIDA PELO ALUNO MARCIO CRISTIANO MONTEIRO E ORIENTADA PELO PROF. DR. JULIANO ALVES BONACIN.

CAMPINAS
2016

Agência(s) de fomento e nº(s) de processo(s): CAPES

Ficha catalográfica
Universidade Estadual de Campinas
Biblioteca do Instituto de Química
Camila Barleta Fullin - CRB 8462

M775s

Monteiro, Marcio Cristiano, 1989-
Study of the properties of Prussian blue obtained via $[Fe(CN)_5(mpz)]^{2-}$ complex / Marcio Cristiano Monteiro. – Campinas, SP : [s.n.], 2016.

Orientador: Juliano Alves Bonacin.
Dissertação (mestrado) – Universidade Estadual de Campinas, Instituto de Química.

1. Azul da Prússia. 2. Cianoferrato. 3. Sensor eletroquímico. I. Bonacin, Juliano Alves,1980-. II. Universidade Estadual de Campinas. Instituto de Química. III. Título.

Informações para Biblioteca Digital

Título em outro idioma: Estudo das propriedades do azul da Prússia obtido através do complexo $[Fe(CN)_5(mpz)]^{2}$**Palavras-chave em inglês:**
Prussian blue
Cyanoferrate
Electrochemical sensor
Área de concentração: Química Inorgânica
Titulação: Mestre em Química na área de Química Inorgânica
Banca examinadora:
Juliano Alves Bonacin [Orientador]
Anamaria Dias Pereira Alexiou
André Luiz Barbosa Formiga
Data de defesa: 26-07-2016
Programa de Pós-Graduação: Química

BANCA EXAMINADORA

Prof. Dr. Juliano Alves Bonacin (Orientador)

Profa. Dra. Anamaria Dias Pereira Alexiou (Univ. Mackenzie-SP)

Prof. Dr. André Luiz Barbosa Formiga (IQ-UNICAMP)

A Ata da defesa com as respectivas assinaturas dos membros encontra-se no processo de vida acadêmica do(a) aluno(a).

Este exemplar corresponde à redação final da Dissertação de Mestrado defendida pelo aluno **MARCIO CRISTIANO MONTEIRO**, aprovada pela Comissão Julgadora em 26 de julho de 2016.

Aos meus pais, Efigênia e Valdir

À minha irmã, Márcia

E aos meus amigos, Bruno, Kalil, Pãmyla e Vera,

por toda a ajuda nestes 2 anos de trabalho.

"*A ciência nunca resolve um problema sem criar pelo menos outros dez*".

George Bernard Shaw

ACKNOWLEDGEMENTS

Decidi escrever os agradecimentos em português por ser a minha língua mãe, além de possuir um vasto vocábulo que me permite expressar um pouco da gratidão a cada um(a) abaixo mencionado(a):

À minha mãe, que fez o que pôde e o que não pôde desde o processo seletivo ao término do Mestrado. Pelas ligações para saber como eu estava, quando iria visitá-la e quando eu não tinha aula (mesmo eu explicando que no Mestrado há poucas disciplinas)...

Ao meu pai, que me ajudou e muito com processos burocráticos referentes à estadia em Campinas. Pelas visitas recebidas e dadas nos momentos em que retornava à Viçosa e pela mudança positiva que tem mostrado nos últimos anos...

À minha irmã, que presenciou cada detalhe desta minha aventura MG-SP. Pela amizade e idiotices que sempre fazemos questão de permanecer. Por sempre termos que responder que não somos gêmeos e que o nome igual é culpa dela...

Ao meu avô, que infelizmente não esteve presente nesta minha conquista, mas que ansiava o meu retorno desde a minha ida à Portugal.

À minha avó, que sempre quer todos os netos por perto, rezando para que o tempo passasse logo, para que então eu possa retornar para seus afetuosos abraços.

Ao Professor Efraim, que me auxiliou com as burocracias para a efetivação da matrícula.

Aos Professores Portugueses e Brasileiros da graduação, que contribuíram para a minha formação.

À Aime, que sempre esteve presente e ouviu minhas vibrações e lamentações. Que me emprestou a casa da mãe dela até que eu pudesse me mudar para Campinas. Pela amizade e panguazice ao responder coisas como “quem mais que é besta?” e “que ano é hoje?”.

À Neize, mãe da Aime, por ceder um espacinho em sua residência enquanto não conseguia me mudar para Campinas.

Às meninas da CPG, Bel, Gabriela, Isabela e Janáina. Pelas amolações ao longo desses dois anos, brincadeiras, ajudas, papéis e mais papéis!

Ao meu Orientador, Juliano, pela disponibilidade, paciência, aprendizado e compromisso com a Ciência.

Aos técnicos do Instituto de Química, em especial à Cláudia e sua ajudante, Tatiane, e Sônia. Pelo bom humor, ajuda e disponibilidade.

À minha madinha, Dani, pelas ligações e conversas, principalmente no inicio do curso.

Ao meu amigo, Eduardo, pelas conversas, discussões, jogatinas e filmes. Por ter sido como um irmão e feito muito por mim.

Aos pais do Eduardo, Cecília e Roberto, por me hospedarem ocasionalmente e me receberem de braços abertos.

Ao pessoal do Grupo LNanoMol. Morandi, por toda a ajuda, principalmente no inicio do Mestrado. Kalio, pela quase coorientação, contribuindo para elaboração, execução e discussão de dados. Pãmylinha, pelas inúmeras ajudas concedidas, desde caronas, pinturas de parede à experimentos, materiais de estudos e edições de figuras. Vera, pelas brigas, gritos, palavras e expressões novas (preocupança, câncero, esticlete, absurdo caro etc), inglês, MEV e experimentos. René, pelas sínteses e RMNs, tentativas de conversas em inglês e churrascos. Flavinha, pelas conversas e reclamações ouvidas, além de problemas similares no decorrer dos experimentos. Nosso vagabundinho, Lucas, pelas discussões do projeto e ajuda na execução de experimentos e preparo de soluções. E Joice, pelas conversas no fim de todo o processo.

À galera dramática do Preeeeekini! Ana, pelos estudos simétricos e assimétricos, conversas sem fim, músicas em marciano (uu du uutru plunutu), brincadeiras do deserto e pressas sem um motivo aparente. Dogi, pelas conversas de games, de Química, pelos lanches na Sapore e Mc Donalds e pela grande ajuda na escrita desta dissertação. Sabrila, pelas conversas, jogos de Mario e falta de sorte. Aos já citados, Morandi, Kalio, Pamylinha e Vera que também constituem este grupo. A todos, também, pelos momentos pós-laboratório. Momentos esses que proporcionaram inúmeras risadas, dramas, gastos, jogos e mais dramas!

Aos agregados do grupo: Danijela, Enoque, Luciano, Marcos (Dotô), Marjorie e Thiago, que normalmente estão presentes nas saídas que envolvem bares, churrasco ou jogos e que contribuem para mais drama e diversão.

Aos jogos bastante usufruídos por nós: Munchkin, Seven Wonders, Wii, Pokémon e alguns outros. Por nos proporcionar horas de diversão (e claro, drama).

À Rafa e ao Ramon, por me aturarem nas visitas frequentes. Além da primeira, por me drogar com lasanha de berinjela e o segundo, por emprestar o carro para escapadas para o cinema, Sergel ou para o próprio laboratório, em dias de chuva.

À galera que estava e/ou está no laboratório: Augusto, Carlos, Prof. Corbi, Prof. Diego, Prof. Formiga, Eduardo, Fernando, Helen, Irlene, Julia, Luis, Marcos (chupa galo!), Mariana, Naheed, Nina, Renan, Sérgio e Thalita. Pelas conversas acadêmicas e não acadêmicas, pelos bolos e pela ajuda.

Aos técnicos do laboratório, Cíntia e Bili, e às ajudantes dos técnicos, Babi e Luana, pelas diversas ajudas relacionadas ao laboratório e também pelas conversas.

Às esquerdistas, Andreza, Gabi, Néia, Paty e Rayane, pelas conversas em texto e também em voz, quando nos encontrávamos por Viçosa. Pelas zoações, diversão, assim como papos de químicos.

À TS, Welton e Danilo. Pelas conversas ao longo desse tempo, sobretudo reclamações, papo sério e conversa fiada.

Ao Piadas Nerds, que me proporcionou conhecer pessoas incríveis e nerds! Em especial ao Ivó, Luizim, Kilgrave, Leh, pH, ShEllder, Siri, VM e Allan. O passeio em SP foi 01100100 01100101 01111010!

Ao Fleups, pelas brejas em Campinas, quando tivemos oportunidade. É muito bacana poder conhecer alguém que se conhecia, através de jogos, desde mais de 5 anos!

Ao Rick, pelas caçadas de Hellspawn, que deu lucro, passou tempo, desestressou e matou saudade do amiguinho. ;*

Ao Iwyson, que me aturou bastante no final do Mestrado e pode me ajudar a seguir em frente, principalmente rindo dele se irritar comigo. Trouxa! Hahaha.

Aos Professores Camila, Formiga e Anamaria, por participarem da minha qualificação e/ou defesa, além de contribuírem para o meu trabalho e crescimento profissional.

Aos Professores, Ana Flávia, Corbi, Formiga e Kubota, pelo aprendizado em suas respectivas disciplinas.

Aos alunos das turmas que participei como PED, ao Arnaldo, Ana, Dogi e Luis, onde pude aprender, ajudar e ser ajudado nos conteúdos de Química Inorgânica.

À Mari, Aime e demais colegas do laboratório, por terem assistido à minha apresentação da Defesa.

Aos meus parentes, amigos e vizinhos, que torceram por mim. Em especial:

À minha Tia Aparecida, ao meu Tio João (que infelizmente não está entre nós) e meus primos Jaque, Jú e Gio. Pela presença em praticamente todas as minhas idas à Viçosa. Pelos almoços e conversas agradáveis.

À minha Tia Luciane, ao meu tio Carlinho (que infelizmente não está entre nós) e meus primos Diego, Isabela e Rafaela. Pelas conversas, comilanças e palhaçadas.

Aos meus primos Beto e Camila. Pelas jogatinas de Mario Kart acompanhadas de Suco Gummy (Arriba! Abajo! Al Centro! Adentro! Ai ai ai!) #FestaNaCasaDaPaula.

A todos vocês, que de alguma forma contribuíram para o meu crescimento ao longo desses dois anos, os meus mais sinceros agradecimentos.

RESUMO

Neste trabalho, foram realizados estudos sobre o complexo pentacianido(N-metilpirazínio)ferrato(II) $[Fe(CN)_5(mpz)]^{2-}$ (mpz = metilpirazínio) e o seu azul da Prússia (PB-mpz). As caracterizações dos compostos foram realizadas através de espectroscopia eletrônica (UV-Vis) e vibracional (FT-IR), espectroeletroquímica, voltametria cíclica e RMN. Análises eletroquímicas mostraram um aumento de reversibilidade do processo de redução do ligante mpz, ao se coordenar ao ferro, além da dependência do pH do meio. Também é mostrado que a troca do ligante amino pelo mpz aumenta o potencial de oxidação do metal. Experimentos de estabilidade do complexo em tampões revelam estabilidade em baixos valores de pH. A substituição do ligante por dimetilsulfóxido ocorre por mecanismo dissociativo, com uma constante de dissociação de 3,78 x 10^{-4} s^{-1}. Os dados obtidos para o PB-mpz foram comparados ao azul da Prússia tradicional (PB), onde os seus espectros eletrônico e vibracional apresentam bandas características tanto do pentacianidoferrato(II), quanto do PB. Os voltamogramas cíclicos mostram um deslocamento do potencial de redução do ligante e de oxidação dos ferros presentes na estrutura. O método de Job foi utilizado para determinar a estequiometria do PB e PB-mpz de acordo com a quantidade de íons ferro(III) e complexo de ferro(II). O PB possui a proporção de 1:1 (Fe^{3+}:$[Fe(CN)_6]^{4-}$), enquanto o PB-mpz tem proporção de 1:2 (Fe^{3+}:$[Fe(CN)_5(mpz)]^{2-}$). Dados de DRX sugerem baixa cristalinidade para o PB-mpz. Por fim, eletrodos modificados com filme de PB-mpz foram utilizados como sensores eletroquímicos para H_2O_2, apresentando resposta linear na determinação deste analito.

ABSTRACT

In this work, studies of pentacyanido(N-methylpyrazinium)ferrate(II) $[Fe(CN)_5(mpz)]^{2-}$ (mpz = methylpyrazinium) and its Prussian blue (PB-mpz) were performed. The characterizations of the compounds were carried out by electronic (UV-Vis) and vibrational (IR) spectroscopies, spectroelectrochemistry, voltammetry and NMR. Electrochemical measurements showed an increase of reversibility of the reduction process of the mpz ligand when coordinated to the iron complex, with pH dependence. It was also found that the ligand exchange between NH_3 and mpz increased the oxidation potential of the metal. Experiments of the complex's stability in buffer solution showed that it has a good stability at low pH values. Substitution reaction using dimethyl sulfoxide occurs via dissociative mechanism with dissociation constant of 3.78×10^{-4} s^{-1}. Data obtained for PB-mpz were compared with traditional Prussian blue (PB). Electronic and vibrational spectra showed characteristic bands of pentacyanidoferrate(II) and PB. Cyclic voltammograms revealed a shift of the reduction potential of the ligand and oxidation potential of the iron atoms in PB-mpz structure. Job's method was used in order to determinate the stoichiometry of PB and PB-mpz according to iron(III) ion and iron(II) complex content. PB has the proportion of 1:1 (Fe^{3+}:$[Fe(CN)_6]^{4-}$), on the other hand PB-mpz has the stoichiometry of 1:2 (Fe^{3+}:$[Fe(CN)_5(mpz)]^{2-}$). XRD data indicated low crystallinity for PB-mpz compound. Finally, chemically modified electrodes by PB-mpz were used as electrochemical sensor of H_2O_2, with a linear response in the determination of this analyte.

SUMMARY

1. INTRODUCTION

1.1. Overview

Pentacyanidoferrate(II) complexes (PCF) coordinated to N-heterocyclic groups have been extensively studied[1]. Cyanide ligands in these complexes are inert in the substitution reactions. In general, the literature concerning these complexes describes their reactivity, kinetic, spectroscopic and electronic properties based on the modulation caused by other ligands[2].

The study of the pentacyanidoferrate(II) complexes gained importance in the 1970's and were developed by pioneer research of Toma and Malin[3]. These complexes have great affinity for N-heterocyclic compounds, amino acids, sulfoxides, tioethers and tioamines[4]. The modification of PCF by different ligands allows control of their reactivity and facilitates its integration with other chemical systems. Such complexes are relatively stable and are frequently used in studies of: i) mimetic mechanisms of biological systems[5], ii) photochemical mechanisms using the ligand field approach[6], iii) mechanisms of electron transfer and intervalence behavior[7], iv) the modification of gold nanoparticles[4], v) the capacity to form molecular bridges and produce Prussian blue and related structures[8].

PCF may also be used as a precursor of Prussian blue (PB)[9], an inorganic polymeric compound ($Fe_4[Fe(CN)_6]_3.xH_2O$; Fe^{3+} and Fe^{2+}, respectively) with remarkable magnetic, electrochromic and electrochemical properties. PB is highly insoluble and it can be easily prepared by the mixture of iron(III) and pentacyanidoferrate(II).

PB was the first coordination compound synthesized and it is an important pigment for paints and varnishes. In this inorganic compound, Fe^{2+} and Fe^{3+} ions are alternatively distributed in the cubic face-centered structure, surrounded by carbon and nitrogen atoms, respectively[10]. A representation of PB unit cell is presented in **Figure 1a**.

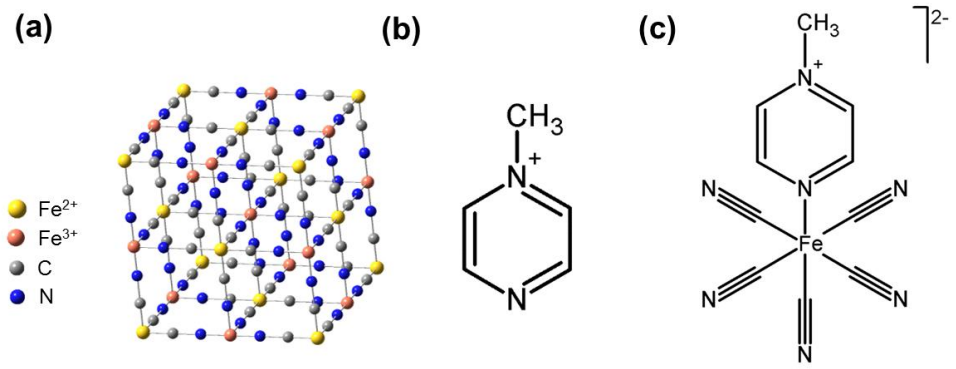

Figure 1. (a) Representations of the unit cell of Prussian blue; (b) N-methylpyrazinium and (c) PCF-methylpyrazinium structures.

PB is a coordination polymer with mixed valence and its intense color is the result of a charge transfer transition (intervalence charge transfer) between the ions $Fe^{2+} \rightarrow Fe^{3+}$ mediated by the cyanide bridges[10b] The versatility of PB is due to its different oxidation states, where the oxidized form is represented as $Fe^{III}[Fe^{III}(CN)_6]$ and the reduced form as $K_2[Fe^{II}Fe^{II}(CN)_6]$, named Berlin green and Prussian white, respectively[11].

This inorganic compound is also a semiconductor and its ferrimagnetism is associated with the electronic delocalization in the ground state between Fe^{2+} and Fe^{3+} ions[12]. Due to its electronic, structural and electrochemical properties, PB has been used as material for hydrogen storage[13], cathode of fuel cells[14] and mainly in electrochemical sensors for analytes like ascorbic acid, hydrogen peroxide and glucose[9, 11, 15]. In the scenario of numerous applications using Prussian blue, the key for the development of new PB is its synthesis through PCF complexes.

For this purpose, the ligand N-methylpyrazinium (mpz, **Figure 1b**) coordinated to PCF is presented as an interesting alternative (**Figure 1c**). Mpz ligand is a very weak σ base (pKa ≈ -6.0), but a good π-acceptor, when compared to others N-heterocycles[16].

Furthermore, using pentacyanidoferrate(II) instead of hexacyanidoferrate(II) to produce PB can alter some properties, such as electronic structure, reactivity and technological applications. The use of N-heterocyclic ligand allows a possible integration with other chemical systems. In view of PB synthesis starting from pentacyanidoferrate(II) in a previous work[9],

to determine the influence of the N-heterocyclic group to form PB, a question emerged: does the presence of ligand mpz change the electrocatalytic properties of Prussian blue films? This work was motived by this question.

1.2. N-methylpyrazinium

Coordinated N-heterocyclic compounds have been investigated due to their high electron affinities[17]. Nitrogen of this class of molecules easily coordinates to several metals, allowing studies of electron-transfer processes[3a] and reaction mechanisms[18]. These experiments need to be performed under controlled ionic strength environment and pH lower than 8.0.

The simplest aromatic N-heterocyclic compound with six-membered rings is pyridine (py, **Figure 2a**). Substitution of the carbon atom at the *para* position for a nitrogen atom produces pyrazine (pz) represented in **Figure 2b**. Pz is a highly symmetrical molecule whose interatomic distances and π-electron densities at the carbon atoms are very similar to those of py[19]. On the other hand, while py is a moderately strong base (pK_a = 5.2), pz is an extremely weak base (pK_a = 0.6) and only salts of monoprotonated pyrazinium cation can be isolated[20]. The second pK_a of pz has been estimated to have a negative value (pK_{a2} = -5.6)[21]. Thus, if a nitrogen is methylated, mpz is obtained (**Figure 2c**) and it pK_a will be similar to the pK_{a2} of pz[6, 16]. This property allows one to use mpz at any pH value.

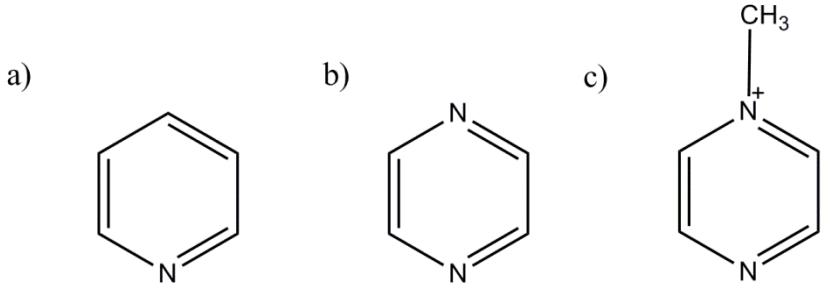

Figure 2. Representations of (a) pyridine; (b) pyrazine and (c) N-methypyrazinium (mpz) structures.

Focusing on N-methylpyrazinium, this compound is an interesting N-heterocyclic that was first synthesized by Bahner and Norton[22]. As it has a

positive charge, it can be electrostatically repelled by the metallic cation. Thus, the unfavorable electrostatic situation from the σ-donor contribution must be overcompensated by a strong back-donation from a metal center rich in electrons to low-lying molecular orbitals of ligand[23]. This affirmation was in agreement with theoretical calculations[24] and experimental data[25], which has shown that mpz receives greater electronic density, when compared with others N-heterocycles. Consequently, this ligand form fairly stable complexes with Fe(II), Ru(II), Os(II), Zn(II) and other metals[3a, 23, 26].

Electrochemical studies about coordinated mpz indicate a reduction process corresponding to the mpz/mpz• couple. Waldhör et al. reported a $E_{1/2}$ value of -0.70 V *versus* Ag/AgCl for the reduction of PCF-mpz measured in 0.1 mol L^{-1} aqueous KCl buffered at pH 7.0 with a glassy carbon working electrode, at a scan rate of 100 mV s^{-1}, but with an irreversible behavior[16]. However, Coe et al. reported a $E_{1/2}$ value of -0.65 *vs* Ag/AgCl for this reduction measured in 0.1 mol L^{-1} aqueous KNO_3 solution at a glassy carbon disk working electrode, at a scan rate of 200 mV s^{-1} and a quasi-reversible behavior[27].

However, electrochemical reduction studies about free mpz in 0.1 mol L^{-1} aqueous KCl solution exhibits irreversible behavior (at slow scan rates) and is discussed in this work. Additionally, no electrochemical studies about the free ligand are detailed and some investigations are discussed in this Master's thesis.

1.3. Pentacyanidoferrates

Cyanide ions coordinate to several transition metals. It is coordinated by carbon atom, because the highest occupied molecular orbital (HOMO) has mainly carbon atom characteristics. In addition, the lowest unoccupied molecular orbital (LUMO) can receive electronic density, stabilizing both high and low oxidation states through σ-donation and π-acceptance behavior (**Figure 3**). This property sets CN^- at the end of the spectrochemical series and results in the formation of low-spin complexes with few exceptions[1]. Among cyanide complexes, the most studied transition metal are those of iron.

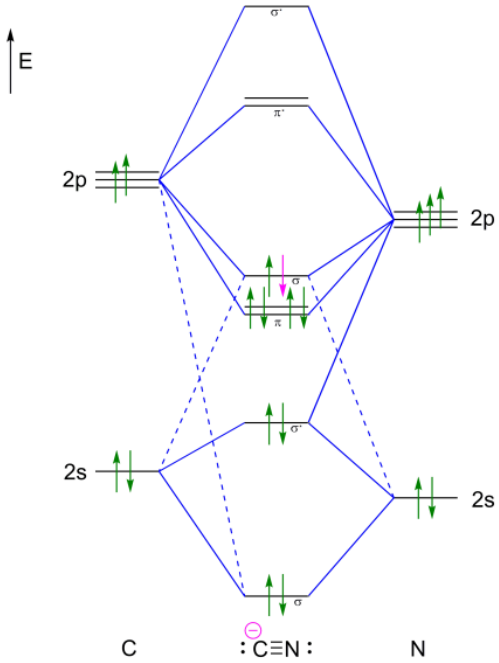

Figure 3. Molecular orbital diagram of cyanide ion.

Iron coordination chemistry is dominated by hexacoordinate complexes[28]. When five of the six ligands are cyanide, the complex is known as pentacyanidoferrate(II) (in agreement to the current IUPAC nomenclature[29]), generically represented by $[Fe(CN)_5L]^{n-}$. L can be a variable number of compounds, like H_2O, NH_3, CO, N-heterocycles, NO, amines, etc.

Hexacyanidoferrate(II) (HCF) and some pentacyanidoferrate(II) (PCF) were described in the literature between 19th and 20th century[30]. Over the years, researches about HCF were increased considerably, while few papers about PCF were published. Before the mid of 20th century, Fluck et al. started to investigate the Mössbauer effect of PCF[31] and the interest of these iron complexes re-emerged. Additionally, Kenney et al. synthesized some PCF coordinated to amines[32]. Moreover, Toma and Malin investigated the chemistry of the pentacyanidoferrates(II) (PCF) to compare to ruthenium complexes[3a]. Later, these authors investigated the mechanism of substitution of PCF[3b], thermodynamic[33] and electrochemical[6] parameters and the nature of metal-ligand bond[17], especially about aromatic nitrogen heterocycles ligands. Furthermore, PCF began to be used to understand isomerization[34] and photochemical[35] reactions, electrochemistry[36], electron transfer reactions[7, 37], bioinorganic systems[38], binuclear complexes[39], modification of gold

nanoparticles[4] and the capacity to form Prussian blue[40] and Prussian blue films[9].

Most of PCF can be prepared from complexes such as hexacyanidoferrate(II) ($[Fe(CN)_6]^{4-}$), nitroprusside ($[Fe(CN)_5(NO)]^{2-}$) or aminnepentacyanidoferrate(II) ($[Fe(CN)_5(NH_3)]^{3-}$), which are commonly presented in the sodium or potassium salt form[3a]. Following the chemical characteristics, PCF can be divided in four classes[41]: a) isoelectronic ligands (NO^+, CO e CN^-); b) phosphorous, sulphur and arsenic donor atoms; c) saturated ligands; and d) nitrogen heterocycles ligands. The last cited class has received a special attention, being the main PCF group studied and the focus of this work.

The striking point of the PCF-heterocycles is the charge transfer transition at the visible part of electromagnetic spectrum, which give these complexes an intense color. HCF complex has a LUMO with high energy and consequently the metal-to-ligand charge transfer (MLCT) transition occurs in the ultraviolet region. However, replacing a N-heterocyclic ligand by a cyanide ion results in a LUMO with lower energy and hence results in a transition in the visible region (**Figure 4**). Thus, spectroscopic and reaction mechanism studies of these complexes instigated the interest of many researchers[3, 34-35].

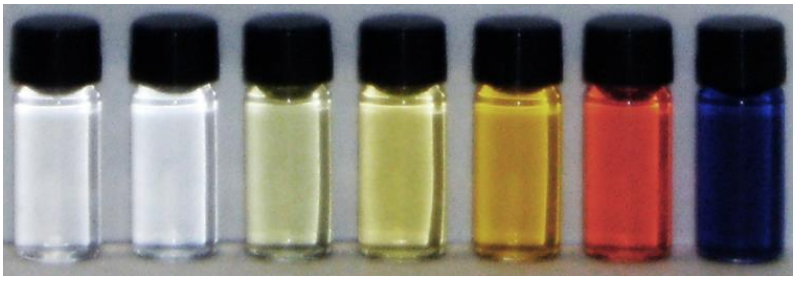

Figure 4. PCF aqueous solutions. From the left to the right: nitro (NO), cyanide (CN^-), aqua (H_2O), ammine (NH_3), isonicotinate ($C_6H_4NO_2$), pyrazine ($C_4H_4N_2$) and methylpyrazinium ($C_5H_7N_2$).

Another important characteristic of cyanide complexes is the ability to form bridging species[1]. This allows the formation of polycyanidometalates known as Prussian blue (PB). Considering the changes in the characteristics of PCF, compared to HCF, it is expected that the corresponding PB of PCF

exhibits different properties than the traditional PB. Hence, the next section introduces this widely studied polymeric coordination compound.

1.4. Prussian blue

1.4.1. History and applications

Ferric hexacyanidoferrate(II) is a coordination compound accidentally discovered by Diesbach and Dippel at the beginning of the 18th century[42]. The name Prussian blue was given for being the dye used in Prussian military uniforms. Chemically, PB can be represented by $KFe^{III}[Fe^{II}(CN)_6]$ or $Fe^{III}_4[Fe^{II}(CN)_6]_3$. This polymeric complex is highly insoluble and it can be synthesized by adding a ferric chloride solution to a potassium hexacyanidoferrate(II) solution.

However, the secret of PB was kept for nearly 20 years. From the date of the first publication until the beginning of the 20th century, about 100 different methods to produce PB were described[43]. In 1782 Scheele discovered hydrogen cyanide by heating PB with sulfuric acid and in 1811, Gay-Lussac concluded that PB contained cyanide[44]. Only in 1936, the first chemical structure was proposed by Keggin and Miles[45], while in 1977 a detailed structure was confirmed by Ludi et al.[46].

Initially, PB was used as a pigment, expanding its applications in the course of time. The high affinity for cations allowed the use of this compound to trap thallium and cesium[47]. Electrochemical properties like electrochromism[48] and catalysis of hydrogen peroxide[49] and molecular oxygen reduction[50] were reported, also. Current investigations are focused on its use in electrochemical sensors[11], fuel cells[51] and sodium batteries[52].

1.4.2. Structure and characteristics

Though PB structure took a long time to be proposed, Davidson distinguished both formulas denominated soluble and insoluble. The term soluble is inappropriate and refers to the ability of PB to form colloidal solutions[53]. Then, the X-ray analysis of PB were performed by Keggin and

Miles[45], identifying a face-centered cubic (FCC) structure, where the soluble form has potassium cation at tetrahedral holes, while the insoluble form has iron(III) cations (**Figure 5**).

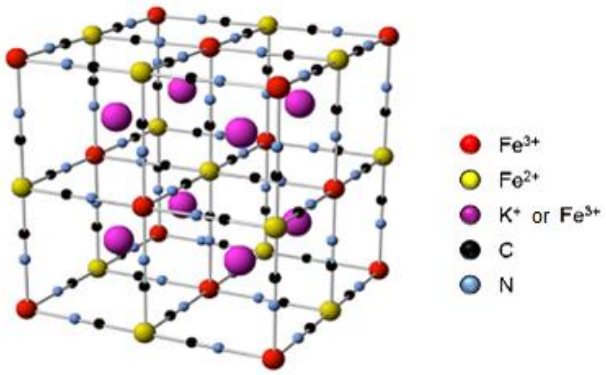

Figure 5. Representation of Prussian blue structure adapted from reference [54].

Moreover, with the contribution of Ludi et al., no iron(III) cations were found inside the FCC structure and the unit formula of PB contained 14 to 15 water molecules[46]. Recent studies concerning the evolution of water dynamics in this complex showed that PB has 14 water molecules and six of them are coordinated to Fe(III), while the other eight are non-coordinated[55].

On the other hand, as a consequence of these structural characteristics (cavities), Prussian blue may contain coprecipitated films or occluded ions, indefinite amounts of water, possibly hydrolyzed cyanidoferrate(II), variable stoichiometry and structural disorder[10b]. Consequently, the exact PB composition was always surrounded by doubts and the obtention of single-crystal is very difficult[56].

Another problem related to PB was about the iron atoms oxidation state in the structure. Most articles appointed two distinct formulas: the reaction of Fe(II) salt and ferricyanido to form Turnbull's blue (TB), as Fe(III) salt and ferrocyanido to form Prussian blue. They believed that the oxidation states of the iron atoms were unknown or indistinguishable. Then, in 1969, Hansen[57] et al. showed three evidences that confirmed the oxidation states of the metals:

a) The electronic spectrum of $KFe[Fe(CN)_6]$ indicates that the salt is ferrocyanido. The characteristic band of the complex can only be

assigned by assuming that the iron atoms surrounded by the carbon are spin-paired-d^6 and that the iron atoms surrounded by the nitrogen are spin-unpaired-d^5 (considering that nitrogen atom is a harder base than carbon atom and iron(III) is a harder acid than iron(II)[58]). **Figure 6a** shows the UV-vis spectrum of PB. The difference of the iron atoms oxidation states allows an intervalence charge transfer ($Fe^{II} \rightarrow Fe^{III}$), responsible for the blue color of PB[59]. Then, the possibility of a resonance form with indistinguishable iron atoms is thus eliminated.

b) Study of the frequency of the C-N stretching. This stretching for the ferrocyanido occurs at a lower frequency (2010-2120 cm^{-1}) and is always sharper and more intense than the equivalent band for ferricyanide (2115-2176 cm^{-1}). **Figure 6b** shows the infrared spectrum of PB. Note that the wavenumber value of C-N stretching appears at range of values for ferrocyanide.

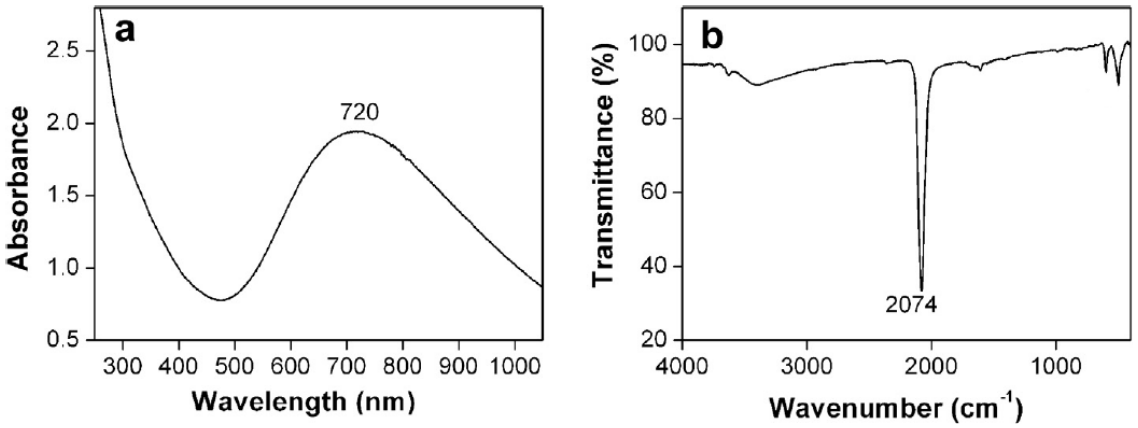

Figure 6. Prussian blue (a) electronic and (b) vibrational spectra. Adapted from reference [49].

c) The description of the electronic configuration of the iron atoms in PB using Mössbauer spectroscopy showed a large quadrupole interaction as well the position of the peak determine the iron atoms in the N-holes to be Fe(III). Also, the iron atom contained in the C-holes were characteristic of spin-paired Fe(II).

Returning to pentacyanidoferrates(II), when their solutions are in contact with aqueous iron(III), the corresponding PB is formed. However, if the ligand is

NO, no PB is formed, due to its non-innocent character[60]. Once the ligand is NH_3 or H_2O, the produced PB is very similar to the ligand CN^- (traditional Prussian blue). When the ligand is an N-heterocycle, the MLCT from PCF is still observed[8], along with the intervalence charge transfer from Fe^{II}-CN-Fe^{III}. Consequently, the PB color may vary (**Figure 7**). Another interesting point is the ligand contribution to form holes in the PB structure. The morphology and crystallinity of the resulting polymers are influenced by the nature of the ligands associated with the PCF[40]. This type of PB can be used to obtain mesoporous materials[61].

Figure 7. PB aqueous solutions. From the left to the right: nitro (NO), cyanide (CN^-), aqua (H_2O), ammine (NH_3), isonicotinate ($C_6H_4NO_2$), pyrazine ($C_4H_4N_2$) and N-methylpyrazinium ($C_5H_7N_2$).

Besides these characteristics, the electrochemical properties of PB are extensively investigated and will receive a special attention in this work. The next topics describe some electrochemical properties, electrode modification and the chemistry of one of the main targets of detection, which is hydrogen peroxide.

1.4.3. Electrochemical properties

When PB is subjected to electrochemical process, the iron atoms can be reduced or oxidized. A typical cyclic voltammogram of a PB modified electrode is shown in **Figure 8**. The reduced form is known as Prussian white (PW, or Everitt's salt) and the oxidized one is Berlin green (BG). However, some authors describe BG as an incomplete oxidized form, while the complete oxidized form is called Prussian yellow (PX, or Prussian brown)[62].

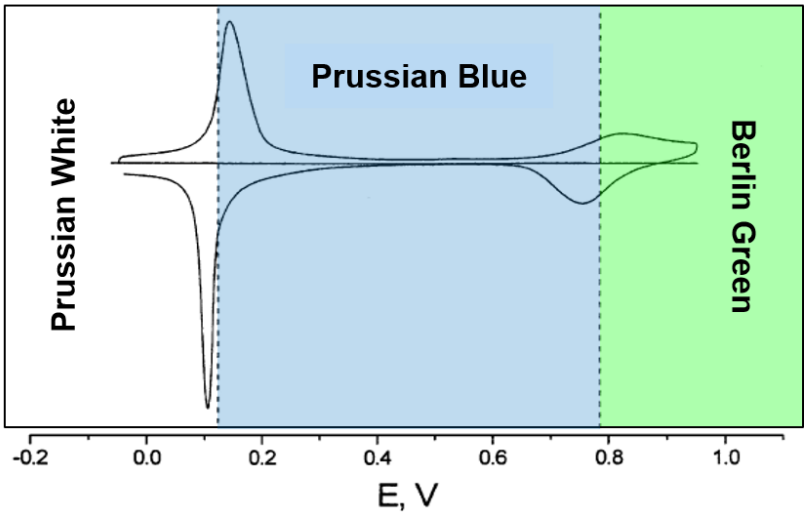

Figure 8. Cyclic voltammogram of Prussian blue modified glassy carbon electrode; 0.1 mol L^{-1} KCl, 40 mV s^{-1}. Adapted from reference [11].

To understand these processes, generally PB is electrodeposited on electrodes[63]. Reduction of PX is the principal electron-transfer process in this deposition (**Equation 1**).

$$\underset{\text{(PX)}}{[Fe^{III}Fe^{III}(CN)_6]} + e^- \rightarrow \underset{\text{(PB)}}{[Fe^{III}Fe^{II}(CN)_6]^-} \quad (\mathbf{1})$$

Due to the negative charge on PB, compensating cations (initially Fe^{3+}, then K^+ of supporting electrolyte) are present in the PB film for electroneutrality[64]. On the other hand, when PB is oxidized again, only partial electrochemical oxidation occurs, yielding BG, represented by **Equation 2**:

$$\underset{\text{(PB)}}{3[Fe^{III}Fe^{II}(CN)_6]^-} \rightarrow \underset{\text{(BG)}}{[Fe^{III}{}_3[Fe^{III}(CN)_6]_2[Fe^{II}(CN)_6]]^-} + 2e^- \quad (\mathbf{2})$$

Only in a really thin film it is possible to form PX again, because the potential to completely oxidize PB is too high, causing the break of the film before PX is formed[62a].

Finally, the reduction of PB yields PW, which is colorless (**Equation 3**). For all redox reactions (**Equations 1**, **2** and **3**), there is a concomitant ion ingress/egress in the films for electroneutrality[64].

$$[Fe^{III}Fe^{II}(CN)_6]^- + e^- \rightarrow [Fe^{II}Fe^{II}(CN)_6]^{2-} \quad (\mathbf{3})$$

(PB) (PW)

These electrochemical properties of PB films were initially studied by Neff[48]. Electrode modification can be used to create selective surfaces that maintain physicochemical characteristics of the modifier[65]. Concerning in Prussian blue electrode modification, the next topic describe some complementary information about PB films and their synthesis.

1.4.4. Prussian blue films

In order to evaluate the electronic spectra of PB films, Mortimer and Rosseinsky observed a blue shift in the band transition (from 730 to 690 nm), and also a width decreasing, after PB/PW and PW/PB oxi-reduction processes (**Figure 9**). Consequently, they suggested that initially the insoluble form of PB was formed and, after several potential cycles, it was converted to the soluble form[63b]. Complementarily, Lundgren and Murray observed a more stable film only if it was previously reduced to PW[66].

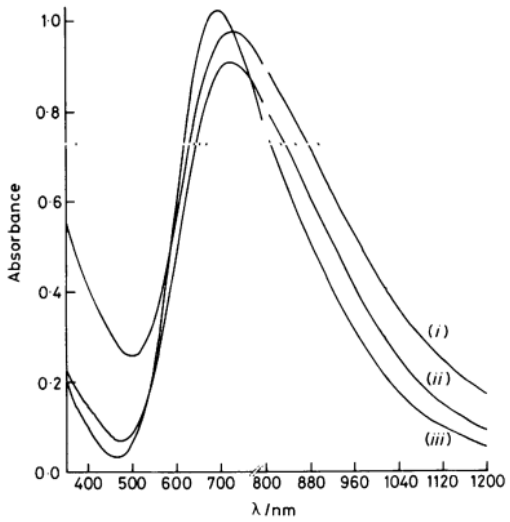

Figure 9. Spectra of PB films under conditions: (i) electrode in dry state after deposition; (ii) in 0.2 mol L^{-1} KCl + 0.01 mol L^{-1} HCl; and (iii) as in (ii) after potential cycling from +0.50 to -0.20 V *vs* SCE at 10 mV s^{-1} in 2 mol L^{-1} KCl. Extracted from reference [63b].

Considering that the insoluble and soluble forms are related to the cations on the cavities of PB, these ions should interfere in the reduction reaction of this polymeric compound. Ozeki[67] et al. reported the cyclic voltammogram behavior using Li^+, K^+, Rb^+ and Cs^+ salts through the cyclic voltammothermometry, in which the electrode reaction heat is measured as well as the current. The heat evolution corresponds to an entropy variation associated to the ions solvation changes. The authors conclude that there is a capacitive current contribution in the presence of potassium. Thus, an intense current peak is presented in the cyclic voltammogram in KCl 0.1 mol L^{-1} (**Figure 10**). Then, a model was proposed to explain this behavior. In this model PB has smaller cavities than PW and K^+ cannot enter in PB structure. Consequently, by reducing the potential, a charge increase on the surface was expected until the system has enough energy to reduce PB. At this point, the cations enter the holes of the film, to maintain the electroneutrality. The current peak corresponds to the sum of faradaic and capacitive current. However, if Rb^+ or Cs^+ are used as the supporting cations, which are smaller hydrated cations, they can enter in the PB lattice at any time. Thus, its capacitance is so large and constant that the accumulated charge is sufficient to reduce PB to PW completely. As a consequence, only faradaic current flows and no intense current peaks are formed.

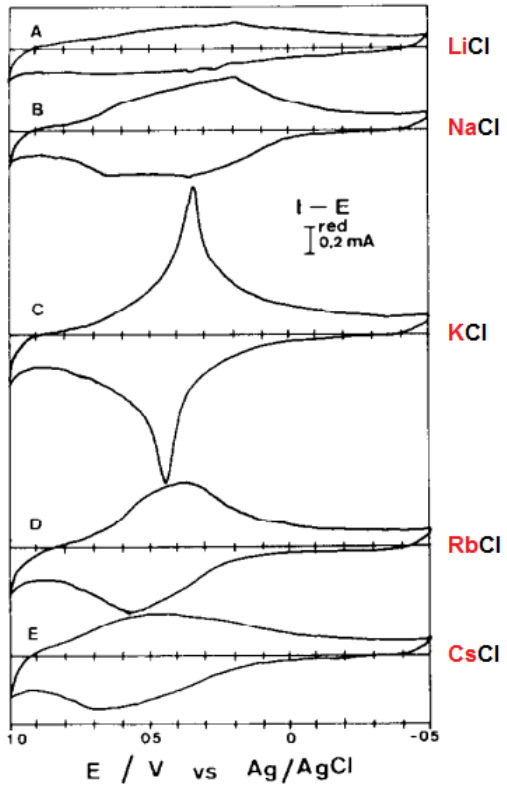

Figure 10. Cyclic voltammograms of PB modified electrode in 0.1 mol L^{-1} (A) LiCl, (B) NaCl, (C) KCl, (D) RbCl and (E) CsCl solutions. Scan rate of 100 mV s^{-1}. Adapted from reference [67].

Additionally, it has been reported that PB film is slowly removed from the electrode surface upon cyclic reduction of the film. This systematic effect is common for all electrolytes. The decrease of the current peak is associated with a loss of ferric iron from the film. Solubilized Fe^{3+} can be detected in the electrolyte solution adding 2,2'-bipyridine (bpy) in the solution, forming a pink color characteristic of $[Fe(bpy)_3]^{3+}$ complex. However, no ferric loss occurs simply upon immersion[66].

There are many ways to modify the surface of the working electrode, which includes dip-coating, electrodeposition, spin-coating, drop-casting, polymeric films, etc.

The deposition method of PB on the electrode, used by Neff, was the immersion of bare electrode in a solution containing $FeCl_3$ and $K_3[Fe(CN)_6]$, until a blue deposit was formed on the electrode surface. This method is known as dip-coating[48]. The deposition solution contains PX that reduces spontaneously to form PB[68].

Afterwards, Itaya et al. synthesized PB films via galvanostatic electrodeposition. The working electrode was immersed in PX solution and cathodically polarized under a galvonostatic condition. Thus, the amount of the PB deposition could be controlled by changing the time of the electrolysis[68]. Since, several researchers have tried to improve the method. Gomathi and Prabakara Rao applied a potential of +1.5 V *vs* NCE in aqueous ferricyanido and ferrocyanido solutions (potentiostatic method). They concluded that at high potentials hydroxyl and carboxyl groups are generated from the electrode surface, changing the localized pH. Consequently, some dissociation of ferrocyanido could occur, releasing Fe(II) ions which would be oxidized to Fe(III) ions at +1.5 V. Then, PB was formed, modifying the glassy carbon electrode[69]. Recently, some improvements of the potentiostatic method were described[70]. After modification, the electrode can be subjected to a series of cyclic voltammetry, which enables a sort of activation of the PB layer, and it can be subjected to a heating step (100 ºC for 1-1.5 h) for the stabilization of the film.

To form PB from PCF complexes, the process is substantially the same. However, the PCF needs to be oxidized. Matsumoto et al. generated the $[Fe^{III}(CN)_5L]$ by adding bromine to the reduced complex in aqueous solution and the excess of oxidant was removed with a vigorous bubbling of argon through the solution. Then, they immersed the electrode into an aqueous solution containing $FeCl_3$, PCF, KCl and HCl, and applied a potential of 0.7 V *vs* SHE for 3 minutes[8]. Pires et al. prepared a solution containing the PCF, KCl, HCl and $K_2S_2O_8$. The solution was stirred for 10 minutes (to oxidize the PCF) and then $FeCl_3$ was added. Thus, PB film was deposited by applying a potential of 0.61 V *vs* Ag/AgCl for 10 minutes[9].

Furthermore, other methods are used and evaluated. A faster and more controlled way, but requiring high cost equipment[71], is the spin-coating method, that involves putting a drop of the solution on the electrode followed by vigorous rotation. Liao[72] et al. synthesized and processed some PB and PB analogues films by layer-by-layer spin-coating method. For each film coating, the compound was spin-coated onto an ITO (indium tin oxide) glass substrate at 600 rpm for 5 s and then at 1500 rpm for another 30 s. Afterwards, the coated film was treated at 120 ºC to accomplish the coating of PB layer. The processes were repeated many times in order to obtain a thicker film.

Another possibility is the drop-casting method, the simplest one. Zhang[73] et al. synthesized chitosan-PB nanocomposites, adding chitosan in a ferricyanido and $FeCl_2$ solution. Then they prepared the modified electrode by dropping 3 μL of chitosan-PB suspension on it. This simple method is useful when the solvent is volatile and it also requires a small amount of the sample. The use of chitosan as stabilizing agent allowed the drop-casting deposition to be employed.

Analogously, Nafion® has been widely used as a protective and selective coating material and as a support for enzyme immobilization. The immobilization of redox mediators (like PB) and co-immobilization of an enzyme and mediator in Nafion membranes have allowed improvement of amperometric biosensors[74].

Despite numerous applications, a significant development of PB-based analytical sensors has been observed during the last 20 years[75]. One of the major roles of such material is in the development of chemical sensors for hydrogen peroxide[76] (**Figure 11**). H_2O_2 is an oxidation product of many enzymatic processes, such the glucose oxidation through the glucose oxidase (GOx). This oxidant is better known for its cytotoxic effects. Increased levels of hydrogen peroxide in cells can result in oxidative stress and cause cellular damage[77]. A strategy to detect this molecule is mimicking the catalytic action of peroxidases using transition metal complexes. These metals show electron transfer process with fast, selective and specific mechanisms. The capacity to catalyze H_2O_2 reduction makes Prussian blue a good redox mediator[76]. Through hydrogen peroxide detection, it is possible to quantify analytes such as glucose, since their concentrations are proportional. Moreover, the current generated by H_2O_2 reduction is proportional to its concentration.

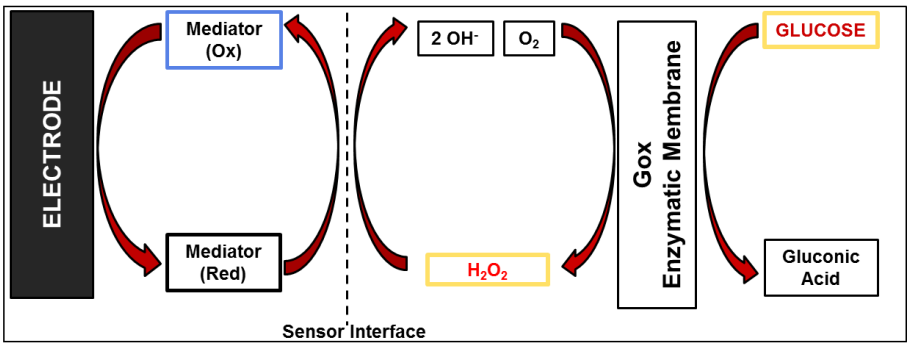

Figure 11. Scheme of a sensor with a redox mediator. A blood sample is placed in a GOx enzymatic membrane and the H_2O_2 produced is reduced by the mediator. Adapted from [78].

To understand the role of hydrogen peroxide in a biological system, it is important to review some chemical characteristics of this analyte. The next topic is focused on that.

1.5. Hydrogen peroxide

Hydrogen peroxide is one of the most versatile existing oxidizing agent. It is superior to chlorine, chlorine dioxide and potassium permanganate. This compound is utilized in environmental monitoring, bleaching in the textile, paper and cellulose. H_2O_2 is also important in monitoring processes in food, medicine, industry, etc[79]. The commonly used methodologies for hydrogen peroxide detection include volumetry[80], spectrophotometry[81], fluorimetry[82], chemiluminescence[83], chromatography[84] and electrochemical methods[49, 75]. The use of electrochemical techniques has shown good selectivity and sensibility, wide range of detection and fast response of the electrode[79].

Hydrogen peroxide is thermodynamically unstable and decomposes to water and oxygen. The rate of decomposition increases with rising temperature, concentration and pH. Haber and Weiss[85] examined the catalytic properties of iron salts to decompose H_2O_2 and the formation of free radicals such as HO• and HOO•.

The electrochemical properties of this compound are well described in the literature. Lingane and Lingane[86] investigated the electrochemical oxidation

of hydrogen peroxide at platinum electrode. The oxidation of H_2O_2 was considered to occur according to the **Equations 4**-**6**:

$$Pt(OH)_2 + H_2O_2 \rightarrow Pt + 2H_2O + O_2 \quad (\mathbf{4})$$

$$Pt + 2H_2O \rightarrow Pt(OH)_2 + 2e^- + 2H^+ \quad (\mathbf{5})$$

$$H_2O_2 \rightarrow 2H^+ + O_2 + 2e^- \quad (\mathbf{6})$$

The hydrogen peroxide reduces the metal hydroxide film to the metal, which is re-oxidized electrochemically. On the other hand, H_2O_2 can be decomposed electrochemically by reduction (**Equation 7**). This process is irreversible and high potentials are involved. The presence of a metallic catalyst can accelerate the decomposition, generating O_2 and/or M-O, which are susceptible to reduction[87]. Vazquez[88] et al. investigated the electrochemical reduction of hydrogen peroxide on polycrystalline copper. The authors have observed that Cu_2O can be reoxidized to CuO by H_2O_2 in a potential interval where CuO is readily reduced (**Equation 8** and **9**).

$$H_2O_2 + 2H^+ + 2e^- \rightarrow 2H_2O \quad (\mathbf{7})$$

$$Cu_2O + H_2O_2 \rightarrow 2CuO + H_2O \quad (\mathbf{8})$$

$$2CuO + H_2O + 2e^- \rightarrow Cu_2O + 2OH^- \quad (\mathbf{9})$$

The possibility for selective detection of hydrogen peroxide by its reduction using PB modified electrodes was first demonstrated by Karyakin et al., who used electrochemical deposition of Prussian blue via cyclic voltammetry[89]. The two kinds of electron transfer processes in PB are due to high-spin $Fe^{3+/2+}$ ion and low-spin $Fe(CN)_6^{3-/4-}$ ion-based redox catalysis for the reduction and oxidation of H_2O_2, respectively. Moreover, due to its high activity and selectivity towards the reduction of hydrogen peroxide, PB is usually considered an artificial peroxidase. A lower overpotential and a very rapid catalytic rate to reduce H_2O_2, makes PB a promising compound for the sensing

application in real samples. This lower overpotential excludes interference from coexisting substances (such as ascorbic and uric acid).

Nowadays, several PB-based electrode modifications are found in the literature[90]. Kong et al. have reported an antenna-like heterostructure of PB head/TiO_2 nanowire arm arrays for interfacial sensing of H_2O_2. While PB reduces the analyte, TiO_2 nanowires provide efficient charge transport towards the electrode substrate. This electrode modification exhibited substantial enhanced electrocatalytic activity and sensitivity for H_2O_2, including a low detection limit (~20 nM), broad detection range (10^{-8} to 10^{-5} mol L^{-1}), short response time (~5 s) and long-term biocatalytic activity (up to 6 months)[91].

Therefore, an increasing number of investigations demonstrate a continuous development of these analytical tools. The pursuit for a more stable and robust PB-based modified electrodes is still required[90]. In this work, the one used PCF-mpz in order to produce the corresponding Prussian blue, PB-mpz, some properties have been evaluated.

2. OBJECTIVES

The objectives are evaluate how the complex pentacyanido(N-methylpyrazinium)ferrate(II) affect the structure and reactivity of Prussian blue films and its electrochemical behavior in sensing of molecular targets.

3. EXPERIMENTAL

3.1. Materials

Pyrazine (99%), methyl iodide (99%) and ammonium hydroxide (28% m/v) were purchased from Sigma Aldrich. Ethanol and sodium iodide were purchased from Merck. Sodium hydroxide (97%), HCl (36.5 – 38%), potassium chloride, dimethyl sulfoxide, acetic, boric and phosphoric acid were purchased from Synth. Sodium nitroprusside was purchased from Acros Organics. All other reagents and solvents were used as received, without further purification.

3.2. Experimental Procedure

3.2.1. Synthesis of N-methylpyrazinium iodide – mpz

2.0 g of pyrazine ($C_4H_4N_2$) were dissolved in 10 mL of methyl iodide (CH_3I), which resulted in a light red colored solution. Then, the solution was kept in the dark at room temperature, without stirring for one week, which turned into a yellow solid. This solution was transferred to the rotary evaporator, heated to 60 ºC and 150 mL of ethanol (C_2H_6O) was added until complete dissolution. The solution was filtered while hot and cooled to room temperature. The crystallization was done in an ice bath, forming large yellow needles that were filtered again, with 15 mL of ice-cooled ethanol. The yield was 75%. $C_5H_7N_2I$ (222.03 g mol^{-1}): calc.: C 27.05, H 3.18, N 12.62; found: C 27.00, H 3.27, N 12.60.

3.2.2. Synthesis of pentacyanidoferrates(II)

3.2.2.1. $Na_3[Fe(CN)_5NH_3].3H_2O$ – PCF-amin:

6.0 g of sodium nitroprusside ($Na_2[Fe(CN)_5NO].2H_2O$) were added to 40 mL of ammonium hydroxide (NH_4OH) in an Erlenmeyer flask (250 mL). The flask was stirred until the complete solubilization of sodium nitroprusside. Then, the flask was covered with aluminum foil and cotton was put on its top to allow the exit of gas. The solution was stirred in the dark for 3 hours and the color became dark-yellow. For precipitation, 6.0 g of sodium iodide (NaI) were added and a yellow solid started to deposit on the bottom. 100 mL of ethanol (C_2H_6O) were slowly added to ensure the complete precipitation. The solid was filtered, washed with ethanol, and dried on a vacuum line until constant weight. The yield was 74%. $C_5H_9FeN_6Na_3O_3$ (325.98 g mol^{-1}): calc.: C 18.42, H 2.78, N 25.78; found: C 18.24, H 2.86, N 25.07.

3.2.2.2. $Na_2[Fe(CN)_5(mpz)].4H_2O$ – PCF-mpz:

0.2 g of aminnepentacyanideferrate(II) was dissolved in 1 mL of water and then mixed with 1 mL of solution of the ligand five-fold concentration. The solution was cooled and stirred in the ice bath for 30 minutes, without light. The solution was treated with 1.0 g of NaI and, after complete dissolution, 30 mL of ethanol were added slowly, under intense stirring, until complete precipitation of the complex. The solid was filtered by vacuum pumping, washed with ethanol, dissolved again in a solution of the ligand of two-fold concentration, treated with 1.0 g of NaI, filtered again and kept in a desiccator. The constant weight was obtained after one week of drying. The complex is very hygroscopic. Yield was 86%. $C_{10}H_{15}FeN_7Na_2O_4$ (399.10 g mol^{-1}): calc.: C 30.09, H 3.79, N 24.57; found: C 29.97, H 3.90, N 23.81.

3.2.3. Synthesis of ferric cyanidoferrates(II)

Ferric hexacyanidoferrate(II), known as Prussian blue (PB), and ferric pentacyanidoferrate(II) (PB-mpz), prepared from the complex in study, were synthesized by a direct method[92].

The direct method is a one-step process consisting of mixing a solution of ferric salt and cyanidoferrate(II). A solution of ferric chloride was prepared (3.7 mmol L^{-1}) and then mixed with a solution of hexacyanidoferrate(II) (2.4 mmol L^{-1}) to produce PB. Additionally, 3.7 mmol L^{-1} of ferric chloride were mixed with a solution of PCF-mpz (2.5 mmol L^{-1}) to produce purple-colored PB-mpz. For some experiments the product was precipitated with acetone, filtered and washed with the same solvent.

3.3. Physical measurements

3.3.1. Elemental analyses

Elemental analyses of N-methylpyrazinium and pentacyanidoferrates(II) were performed using a CHNS/O Perkin Elmer 2400 Analyzer.

3.3.2. Proton nuclear magnetic resonance

^{1}H-NMR spectra of the ligand and PCF-mpz were obtained in deuterated water (D_2O), in a Bruker Avance III – 400 MHz (9.4 T) spectrometer.

3.3.3. Electronic spectroscopy

Electronic spectra were obtained on an Agilent 8453 spectrophotometer, using a quartz cuvette with an optical path length of 1 cm. The measurements were performed on 25 ºC, with range from 200 to 1000 nm.

3.3.4. Vibrational spectroscopy

Infrared spectra of the iron complexes and mpz were recorded as KBr pellets in an MB 100 Bomem Spectrometer at a resolution of 2 cm^{-1} in the range of 4000-400 cm^{-1}.

3.3.5. Cyclic Voltammetry

Cyclic voltammograms were obtained on Autolab EcoChemie PGSTAT20 potentiostat by using 0.1 mol L^{-1} potassium chloride (KCl) as supporting electrolyte in all measurements. A glassy carbon electrode was used as working electrode, an Ag/AgCl (in KCl 3 mol L^{-1}) electrode as reference electrode and platinum wire as auxiliary electrode. For each measurement, solutions of the ligand and complexes at concentration 5.0 x 10^{-3} mol L^{-1} were used. All the solutions were deaerated with nitrogen before the measurements. Potential range varies with compound and the scan rates were 25, 50, 100, and 200 mV s^{-1}. Britton-Robinson buffer solutions[93] were used for pH measurements. For determination of rate constant for EC_i mechanism the scan rates were between 12.5 and 55.0 V s^{-1}.

3.3.6. Influence of pH on the stability of PCF-mpz

For studies of influence of pH, solutions of the complex were prepared with concentrations of 1.0 x 10^{-4} mol L^{-1} in Britton-Robinson buffer solutions (pH 2-11). Electronic spectra were obtained every 30 seconds for 10 minutes, on 25 ºC. For these analyses, the spectrophotometer was equipped with a HP 89090A Peltier.

3.3.7. Substitution kinetics of mpz in the presence of DMSO

Kinetics experiments of substitution by dimethyl sulfoxide (DMSO) were performed using the spectrophotometer equipped with a HP 89090A Peltier. Absorbance of the aqueous solutions of PCF-mpz with DMSO 0.5 mol L^{-1} (100 times in excess) were monitored. Spectra were obtained each 30 seconds for 1 hour, on 25 ºC and controlled stirring. The ionic strength was adjusted with sodium chloride 1.0 mol L^{-1}.

3.3.8. Electrode area calculation

To calculate the electrode area, cyclic voltammetry analyses were performed. For each measurement, solutions of hexacyanidoferrate(III)/ hexacyanidoferrate(II) 1.0 x 10^{-2} mol L^{-1} were used as probe. All the solutions were deaerated with nitrogen before the measurements. The scan rates were 10, 25, 50, 100, and 200 mV s^{-1}. Through the **Equation 16** (section the **4.2.4**) electrode area value was obtained.

3.3.9. Electrode modification

Before modification, glassy carbon electrodes were polished in alumina slurry, rinsed with deionized water, washed ultrasonically and cleaned again with deionized water. The electrode modification was done by layer-by-layer drop-casting method. Firstly, 2.5 μL of cyanidoferrate(II) solution (2.5 x 10^{-2} mol L^{-1}) was dropped on the electrode surface and dried for 30 min. Then, 2.5 μL of

ferric chloride solution (2.5 x 10^{-2} mol L^{-1}) was dropped on the cyanidoferrate(II) modified electrode and it was dried again for 30 min. The second layer was the reverse: 2.5 μL of ferric chloride solution (2.5 x 10^{-2} mol L^{-1}) was dropped on the PB-based electrode and dried for 30 min. Then, 2.5 μL of cyanidoferrate(II) solution (2.5 x 10^{-2} mol L^{-1}) was dropped on the PB-based/Fe^{3+} electrode and was put in a desiccator for 24 h. Thus, the synthesis of PB and PB-mpz was done on the electrode surface through HCF and PCF-mpz, respectively. Before using, the electrode was washed with deionized water.

3.3.10. Spectroelectrochemistry

Spectroelectrochemistry data were obtained on DropSens potentiostats and HP Agilent 8453 spectrophotometer. KCl (0.1 mol L^{-1}) was used as supporting electrolyte. A platinum grid electrode was used as working electrode, a calomel saturated electrode as reference electrode and platinum wire as auxiliary electrode. The electrochemical cell had an optical path length of 1 mm.

3.3.11. Determination of Prussian blues composition

Job's method was performed using electronic spectroscopy. Absorbance of the mixture (acidic solution, pH 1.0, 0.25 mmol L^{-1} of PCF-mpz and $FeCl_3$) was recorded varying the volume of reagents (from 0.0 to 3.0 mL). The final volume was constant (3.0 mL), to maintain the sum of concentrations constant, as well.

3.3.12. X-ray diffraction

X-Ray Powder Diffraction analyses were performed with a Shimadzu XRD 7000 diffractometer, with a copper tube operating at 40 kV and 30 mA. The divergence and scatter slits were of 1.0^{o} and the receiving slit was of 0.30 mm. The scanning was performed in the continuous mode, from 5 to 60^{o} and scan speed of 2^{o} min^{-1}.

3.3.13. Ferric pentacyanidoferrates(II) in the presence of salt solutions

PB and PM-mpz solutions were prepared with cyanidoferrate(II) and ferric chloride equimolar solutions (5.0 x 10^{-3} mol L^{-1}). Sodium acetate ($NaC_2H_3O_2$), sodium borate ($Na_2B_4O_7$), sodium phosphate (NaH_2PO_4), sodium sulfate (Na_2SO_4) and ferric chloride solutions (0.1 mol L^{-1}) were prepared individually. For each compound (PB, PB-mpz and $FeCl_3$) a proportion of salt (acetate, phosphate and sulfate) and deionized water was established, with 1:2:3 ratios, respectively. Thus, electronic spectra data were collected.

3.3.14. The stability of Prussian blues modified electrodes

After modification, the electrodes were submitted to 25 cycles, removed from solution for 10 minutes and submitted to 100 more cycles. They were cycled with both Britton-Robinson and HCl-KCl buffer solutions (pH 2.0), separately. KCl 0.1 mol L^{-1} was used as supporting electrolyte and the scan rate was 50 mV s^{-1} for both cycles (potential range from -0.2 to 0.55 V).

3.3.15. Determination of electrochemical reduction potential of H_2O_2

Before one cycle, 20 μL of H_2O_2 (0.1 mol L^{-1}) was added to HCl-KCl buffer solution (pH 2.0). After 1 minute another 20 μL of H_2O_2 (0.1 mol L^{-1}) was injected. This process was repeated several times. KCl 0.1 mol L^{-1} was used as supporting electrolyte and the scan rate was 50 mV s^{-1} for the cycles (potential range from -0.2 to 0.55 V).

3.3.16. Chronoamperometry

Amperometric response was obtained using 10 mL of HCl-KCl buffer solution and KCl 0.1 mol L^{-1} as supporting electrolyte. The applied potential for the measurement was -0.1 and 0.18 V *vs* Ag/AgCl for PB and PB-mpz films, respectively. After the current stabilization, 20 μL of H_2O_2 (0.1 mol L^{-1}) were added every minute to obtain the analytic curve.

4. RESULTS AND DISCUSSION

4.1. N-methylpyrazinium – mpz

In the following sections data from the mpz ligand are discussed. NMR data has shown the purity, while the spectroscopic (electronic and vibrational) and electrochemical (cyclic voltammetry) were used for the characterization of the ligand. These informations were also used for comparison with the complex and the corresponding Prussian blue. Moreover, the electrochemical behavior of N-methylpyrazinium solution at different pH values and the reaction rate constant of radical mpz also are reported.

4.1.1. Proton Nuclear Magnetic Resonance

The purity of the compound was confirmed via nuclear magnetic resonance (^{1}H-NMR) in deuterated water. **Figure 12** shows the ^{1}H-RMN spectrum, with a peak at 4.53 ppm, correspondent to the hydrogens of the methyl group (H_a), and two other peaks at 9.01 and 9.45 ppm, correspondent to hydrogens of the ring (H_c and H_b, respectively)[94]. Due to the positive charge on the methylated nitrogen, the electron density around the protons H_c increases and they resonate at upper field when compared with protons H_b. The strong absorption at 4.78 ppm is due to residual HOD.

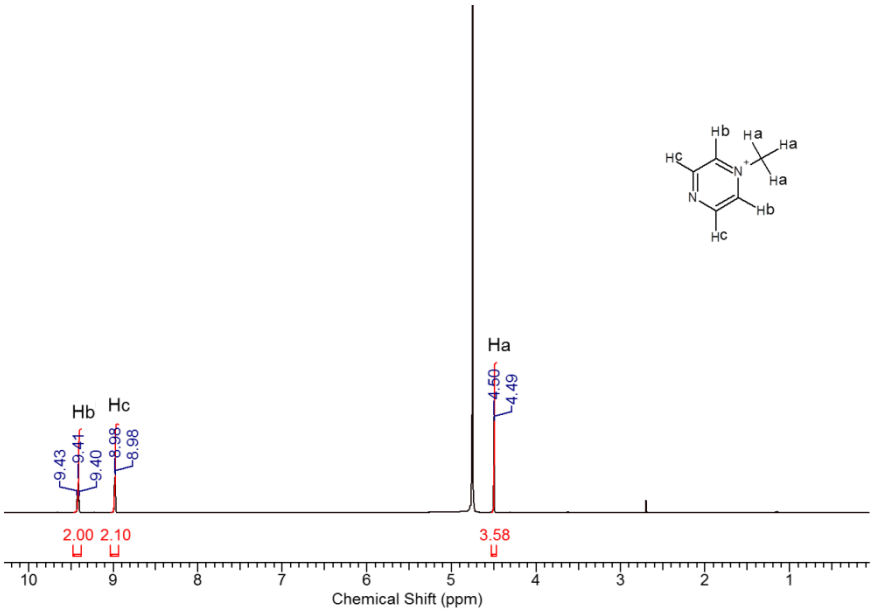

Figure 12. ^{1}H NMR spectrum of mpz in D_2O.

4.1.2. Electronic Spectroscopy

UV-Visible spectrum of the ligand was recorded and it is shown in **Figure 13**. As expected, mpz shows bands in the ultraviolet region of the spectrum. The ultraviolet absorption spectrum of iodide in water at room temperature shows two bands, with a maximum at 193 nm and at 226 nm[95]. The most energetic one could not be shown, due to the limitation of equipment. However, the second one can be seen and is assigned to the charge-transfer-to-solvent transition of free iodide ions. The band at 273 nm is assigned to a π-π* transition of the N-heterocyclic ligand[96].

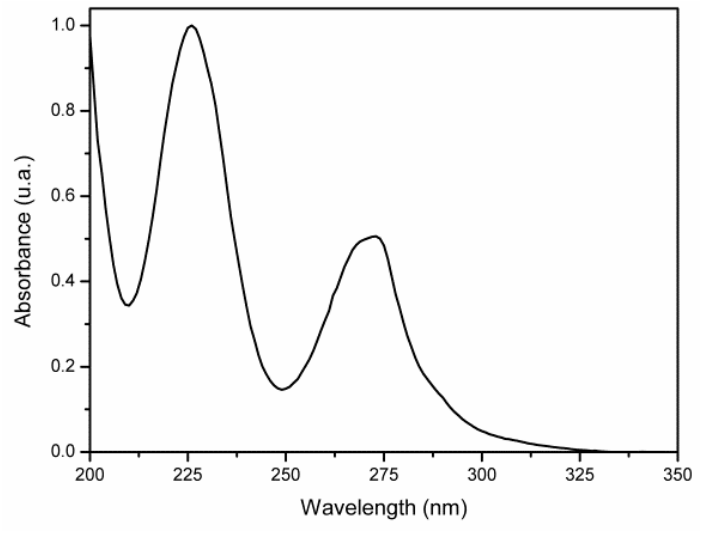

Figure 13. UV-Vis spectrum of N-methylpyrazinium.

4.1.3. Vibrational Spectroscopy

The synthesis of the ligand was also confirmed by vibrational spectroscopy. Corresponding bands and discussion are presented below. The infrared spectrum of mpz is shown in **Figure 14** and observed vibration values are in **Table 1**:

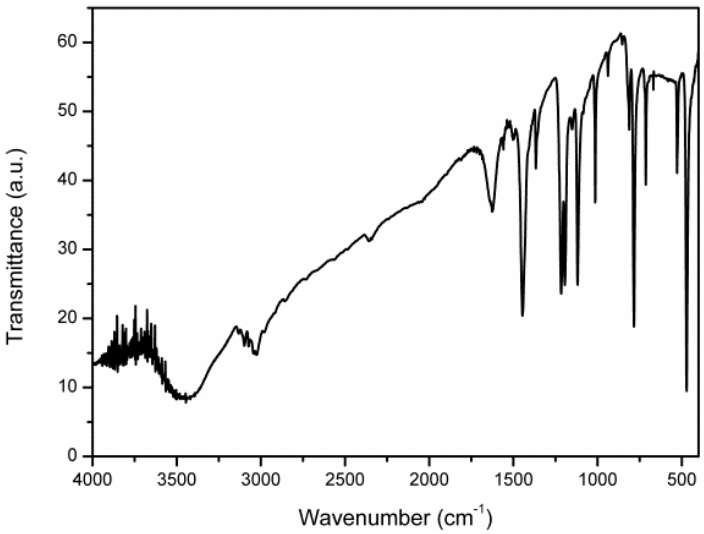

Figure 14. Infrared spectrum of N-methylpyrazinium.

Table 1. Observed infrared bands of N-methylpyrazinium[97].

Wavenumber (cm^{-1})	Assignment
3131, 3098	$\upsilon(CH + CH_3)$
3072, 3042, 3025	$\upsilon(CH)$
1625	$\upsilon(CN_{ring})$
1446	$\upsilon(CC)$
1366, 1216	$\delta(CH)$
1194	ring deformation
1118, 1084, 1013	$\delta(CH)$
938, 811, 784	$\gamma(CH)$
713, 527	ring deformation
470	over plane skeletal bend

υ – stretching; δ – deformation; γ – over plane deformation.

The D_{2h} symmetry of pyrazine molecule is lowered with the addition of a methyl group, and it can be assumed that maximum symmetry of the pyrazinium ion is C_s point group. Pyrazine has 24 symmetry operations, 12 being Raman active, and 10 infrared active. For the C_s point group, there are 36 symmetry operations and all of them become Raman and infrared active. In addition, there are twelve new vibrational degrees of freedom due to the N-CH_3 group. These modes may be mixed with some pyrazine modes and an approximate description of the other pyrazinium symmetry operations is the same as that of pyrazine[97a].

Two important bands of free ligand (**Figure 14**) corresponds to vibrations by methyl group and the CN vibrations in the pyrazinic ring[98], that may confirm the presence of N-methylpyrazinium in the complex, as shown later (see section **4.2.3**). The main band of ring appears at 1194 cm^{-1}, while the bands of methyl group appear at 3098 and 3131 cm^{-1}.

4.1.4. Cyclic Voltammetry

Another technique to characterize the ligand is cyclic voltammetry. Mpz has an interesting electrochemical behavior. In **Figure 15** the voltammograms

of mpz in aqueous solution of KCl 0.1 mol L^{-1} with different scan rates, are shown.

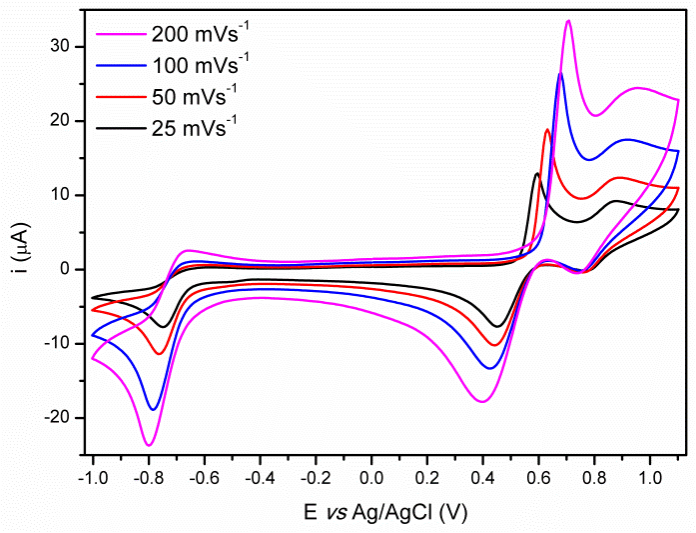

Figure 15. Voltammograms of N-methylpyrazinium in aqueous solution at different scan rates (supporting electrolyte KCl 0.1 mol L^{-1}).

Three process can be seen and are named as R1, for reduction potential ($E_{1/2} \cong$ -0.71 V), O1, for the first oxidation potential ($E_{1/2} \cong$ 0.53 V), and O2, for the second oxidation potential ($E_{1/2} \cong$ 0.83 V). **Table 2** summarizes the potential parameters of these electrochemical processes.

R1 represents reduction of mpz to mpz radical (mpz/mpz•). This reduction shows an irreversible peak at slow scan rates and starts to change the behavior when the scan rate is higher. It can be explained considering that this organic radical is very unstable[16]. Thus, if the scan rate is slow, no mpz• is found at the surface of the electrode when the oxidation potential of this species is reached. However, if the scan rate is increased, there is enough time for the electron transfer process to occur, because some mpz• can enter in contact with the electrode surface.

Table 2. Calculated potential parameters of mpz.

	v (mV s^{-1})	25	50	100	200
R1	E_{ap} (V)	-0.674	-0.688	-0.625	-0.653
	E_{cp} (V)	-0.751	-0.765	-0.786	-0.800
	$E_{1/2}$ (V)	-0.713	-0.727	-0.706	-0.727
	∆Ep (V)	**0.077**	**0.077**	**0.161**	**0.147**
O1	E_{ap} (V)	0.597	0.632	0.681	0.709
	E_{cp} (V)	0.449	0.442	0.428	0.400
	$E_{1/2}$ (V)	0.523	0.537	0.555	0.555
	∆Ep (V)	**0.074**	**0.095**	**0.127**	**0.155**
O2	E_{ap} (V)	0.877	0.891	0.919	0.954
	E_{cp} (V)	0.786	0.758	0.765	0.737
	$E_{1/2}$ (V)	0.832	0.825	0.842	0.846
	∆Ep (V)	**0.091**	**0.133**	**0.154**	**0.217**

It can be seen that the cathodic peak (E_{cp}) of R1 shifts to negative potentials with the increase of the scan rate. On the other hand, the anodic peak (E_{ap}) does not exhibit similar behavior (**Figure 15**, **Table 2**). According to the unstability of the mpz•, the half-wave potential ($E_{1/2}$) is not constant, it is altered with the rate of transport of species to the electrode[99]. Analyzing separation of peak potentials (ΔEp), an increase of the ΔEp occurs when the scan rate shifts from 50 to 100 mV s^{-1} and then a decrease with a scan rate of 200 mV s^{-1}, showing a quasi-reversible behavior at higher scan rates.

O1 and O2 represent oxidation of the iodide ion to triiodide ion (a two-electron step) and oxidation of triiodide ion to iodine (a one-electron step), respectively (**Equation 10** and **11**)[100].

$$6I^- \rightarrow 2I_3^- + 4e- \quad (\mathbf{10})$$

$$2I_3^- \rightarrow 3I_2 + 2e- \quad (\mathbf{11})$$

To prove this affirmation, a cyclic voltammetry of sodium iodide was performed to compare with mpz voltammogram (**Figure 16**). The $E_{1/2}$ of NaI for

the processes O1 and O2, at 100 mV s^{-1}, is 0.445 V and 0.825 V, in this order. The region of these processes is the same, which means a shift to more positive potentials occurs, when the cation is mpz (**Figure 16a**). Additionally, a voltammogram of a solution with NaI and mpz were obtained (**Figure 16b**). The presence of sodium iodide increases the current of the oxidation processes and do not change the current of the reduction process. Finally, some discussion about the electrochemical behavior of O1 and O2 (of **Figure 15**) is presented below.

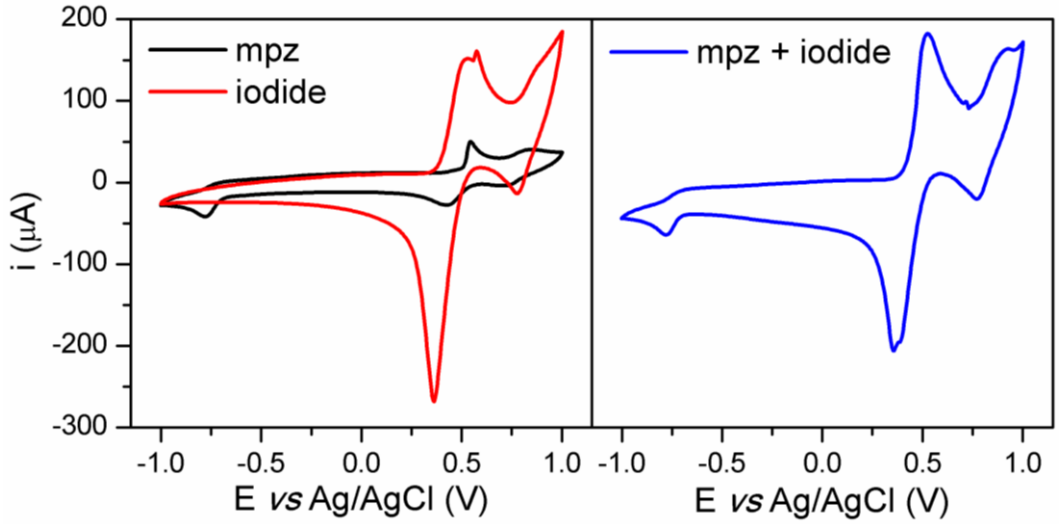

Figure 16. Voltammograms of mpz and sodium iodide (a) in separate solution and (b) in the same solution at 100 mV s^{-1} (supporting electrolyte KCl 0.1 mol L^{-1}).

Both processes exhibit an increase in E_{ap} with the increase of the scan rate, but only O1 decreases proportional with the scan rate, in E_{cp}. Initially ΔEp of both is relatively small and increases with higher scan rates, showing a tendency for an irreversible process. Finally, the $E_{1/2}$ is not the same when the scan rate is altered, as in R1. These results represent a quasi-reversible process for both oxidation processes.

For the three electrochemical processes, a linear variation of the peak current with $v^{1/2}$ is observed (**Figure 17**). This parameter is fundamental and it implies that with an increase in sweep rate there is less time to reach equilibrium at the electrode surface. Consequently, reactions that appears as reversible at slow scan rates can be quasi-reversible at high scan rates[99] (O1 e

O2) or, due to the instability of the formed species (R1) the process may become reversible/quasi-reversible.

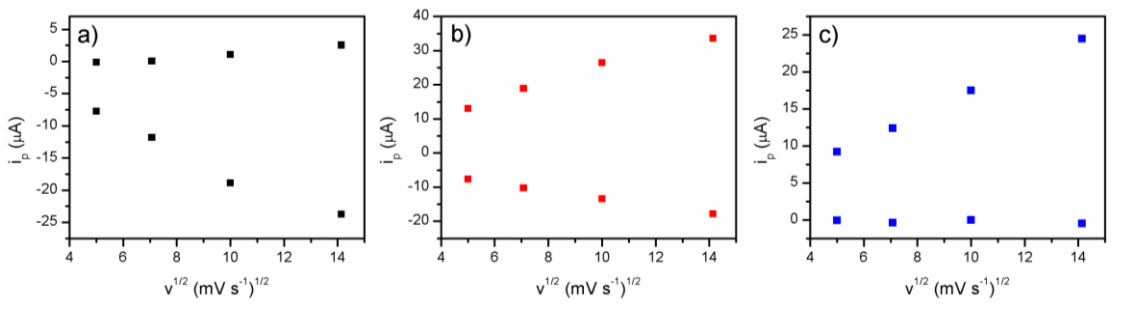

Figure 17. Relation of current peak and sweep rate of the processes: a) R1; b) O1; and c) O2.

Furthermore, from **Figure 15** and **17a**, it is possible to determinate the mechanism of this coupled reaction. Since mpz solutions presents typical behavior of an irreversible process, while higher scans the corresponding anodic peak became visible. This is an indicative of electrolysis product consumption by a homogeneous chemical reaction that follows the electron transfer step (EC_i)[101]. By knowing the mechanism, it is possible to determinate the rate constant of mpz• reaction, discussed in the next topic.

4.1.5. Kinetic of N-methylpyrazinium radical reaction in aqueous media

Considering EC_i mechanism, **Equation 12** and **13** describe the reactions. Increasing the scan rate to values higher than 10 V s^{-1}, the anodic current peak starts to reach half the height of the cathodic current peak. To determinate the pseudo-first-order rate constant (k_f) of the reaction involving mpz• (**Equation 13**), i_{ap}/i_{cp} values of cyclic voltammetry at scan rates between 12.5 and 55 V s^{-1} were plotted against log τ (where τ is the time between $E_{1/2}$ and switching potential, E_λ). Thus, the k_f of the homogeneous chemical process can be determined from Nicholson and Shain treatment of EC_i process[102].

$$mpz + e^- \leftrightarrows mpz\bullet \qquad (\mathbf{12})$$

$$mpz\bullet + A \xrightarrow{k_f} B \qquad (\mathbf{13})$$

Figure 18a shows the work curve, which is characteristic of EC_i process, denoted as case VI by Nicholson and Shain. This work curve relates the rate between the current peaks to $k_f\tau$. Using the average of i_{ap}/i_{ac} values, experimentally obtained, and **Figure 18a**, $k_f\tau$ value is obtained ($k_f\tau = 0.8982$).

Figure 18b shows a linear relationship ($R^2 = 0.9975$) between the experimental values of τ and i_{ap}/i_{ac}. Then, from the equation of straight line of **Figure 18b**, it is possible to obtain τ value ($\tau = 8.956 \times 10^{-3}$ s). Finally, the pseudo-first-order rate constant was calculated by $k_f\tau$ value divided by τ[103] and is estimated as $1.003 \times 10^2\ s^{-1}$.

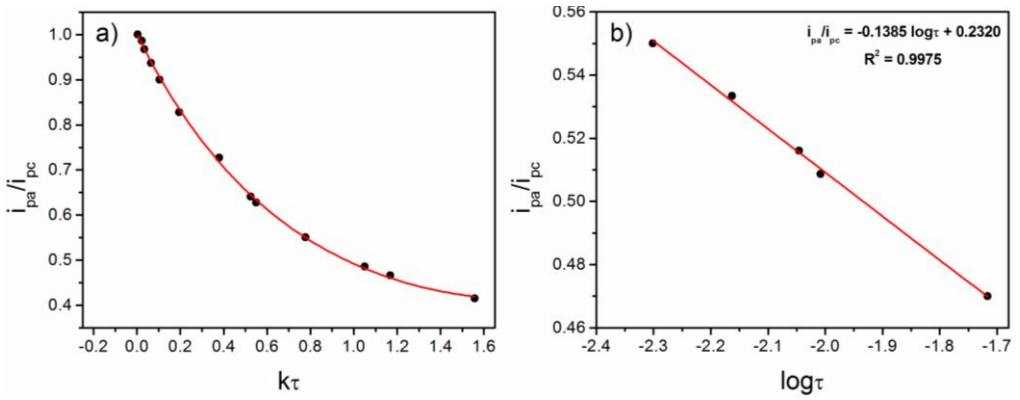

Figure 18. (a) Work curve obtained from [102] and (b) i_{ap}/i_{ac} *vs* log τ plot by cyclic voltammetry data with scan rate from 12.5 to 55 V s^{-1}. τ is the time between $E_{1/2}$ and E_λ.

Although mpz is not protonated in acidic medium[6, 21], the generated species via electrochemical processes (mpz•) needs to be evaluated with the variation of pH values.

4.1.6. Electrochemical behavior of mpz solution at different pH values

Cyclic voltammetric behavior of mpz shows a strong dependence on the pH of the medium (**Figure 19**). The cyclic voltammetry response of mpz at low pH exhibits two redox waves (R1 and R2, where $E_{1/2_{R1}} < E_{1/2_{R2}}$). These

electrochemical processes are not reported in the literature, but an electron spin resonance study has shown that mpz• can be protonated[104]. Thus, at low pH the reduction of mpz occurs at potential $E_{1/2_{R2}}$ and the formed species (mpz•) is rapidly protonated (**Equation 14**). Then, Hmpz• is reduced, may form $Hmpz^{\bullet}_{\bullet}$, similar to dimethylviologen[105] or pair the additional electrons at potential $E_{1/2_{R1}}$.

$$mpz + e^{-} \xrightarrow{H^{+}} Hmpz\bullet \qquad (\mathbf{14})$$

Additionally, the presence of the R2 process appears to become R1 process reversible. With increase of the pH, R2 redox wave could not be observed, showing dependence of the concentration of H^{+}. Consequently, R1 becomes irreversible again.

The two redox waves in positive potentials (O1 and O2) present different behavior, with the increase of pH. While the first one keeps the anodic peak practically unchanged, the second one shifts to more positive potentials. At higher pH, the cathodic peak of both decreases. On the other hand, all these processes shift from quasi-reversible to irreversible when the pH is raised. The formed iodine reacts with hydroxides ions, forming iodate and iodine ions.

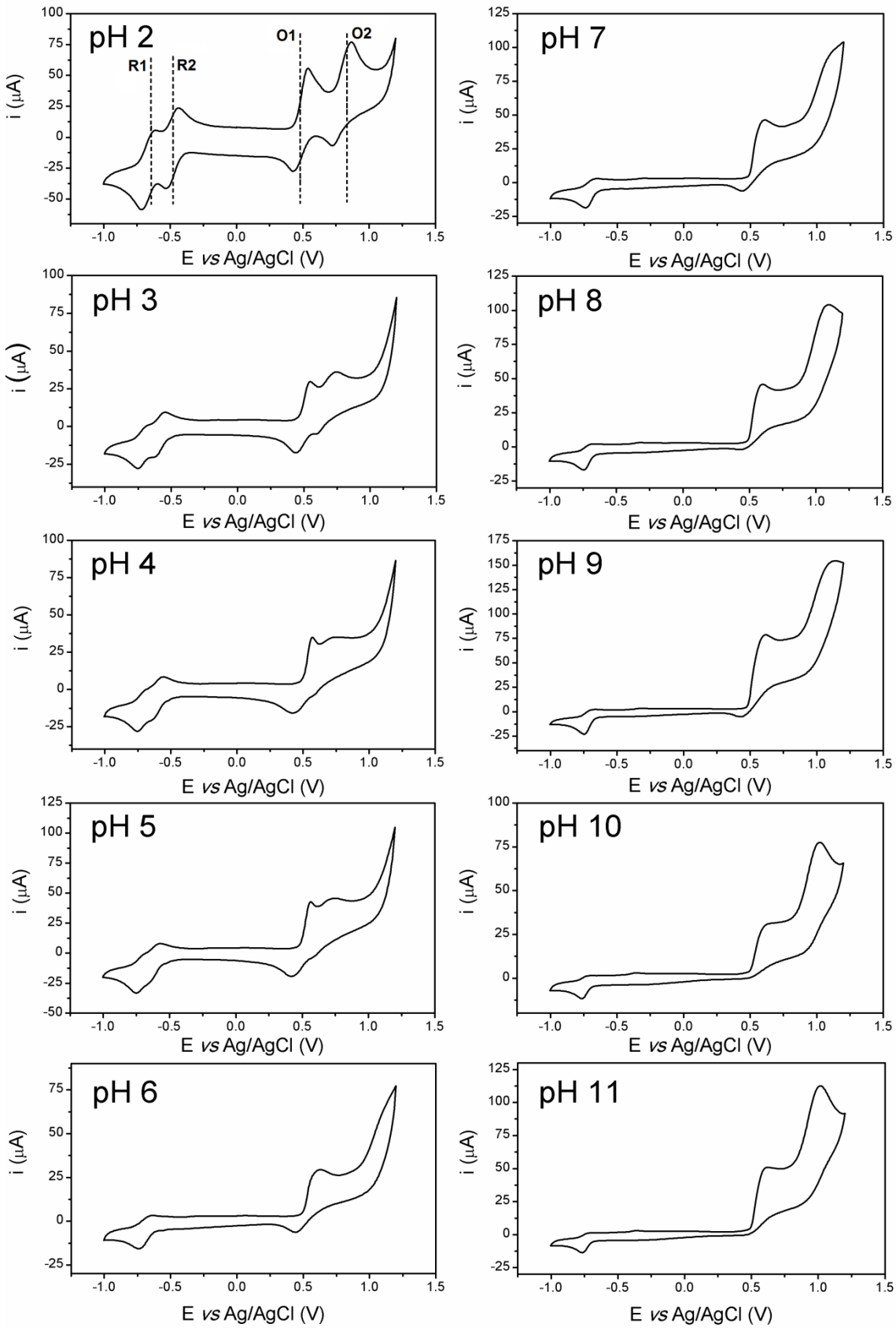

Figure 19. Cyclic voltammograms of mpz in pH 2-11 at scan rate of 100 mV s^{-1}.

4.2. Pentacyanido(N-methylpyrazinium)ferrate(II) – PCF-mpz

After discussing about the ligand, the complex was synthesized and is evaluated in the next topics, organized similar to the section **4.1**: NMR data was obtained to verify the purity, whereas spectroscopy (electronic and vibrational) and electrochemistry (cyclic voltammetry) characterize the pentacyanidoferrate(II) complex. Moreover, the stability and reactivity of PCF-mpz were studied by analyses of electrochemical behavior and electronic spectra of PCF-mpz solutions at different pH values and the substitution kinetics of the mpz ligand in the presence of dimethyl sulfoxide.

4.2.1. Proton Nuclear Magnetic Resonance

^{1}H-NMR spectrum of complex (**Figure 20**) was done in order to compare with the spectrum of the ligand and to confirm the purity. The result showed a signal assigned to the protons from methyl group (H_a) at 4.08 ppm, and the signals of the protons from the pyrazinic ring shift at 8.17 and 9.71 ppm (H_b and H_c, respectively)[94]. The energy of the occupied and free orbitals of mpz are influenced by coordination and the electron density around the protons (H_c) decreases, resulting in a shift to lower fields when comparing with free ligand. The peaks at 3.61 and 1.14 ppm are from residual ethanol.

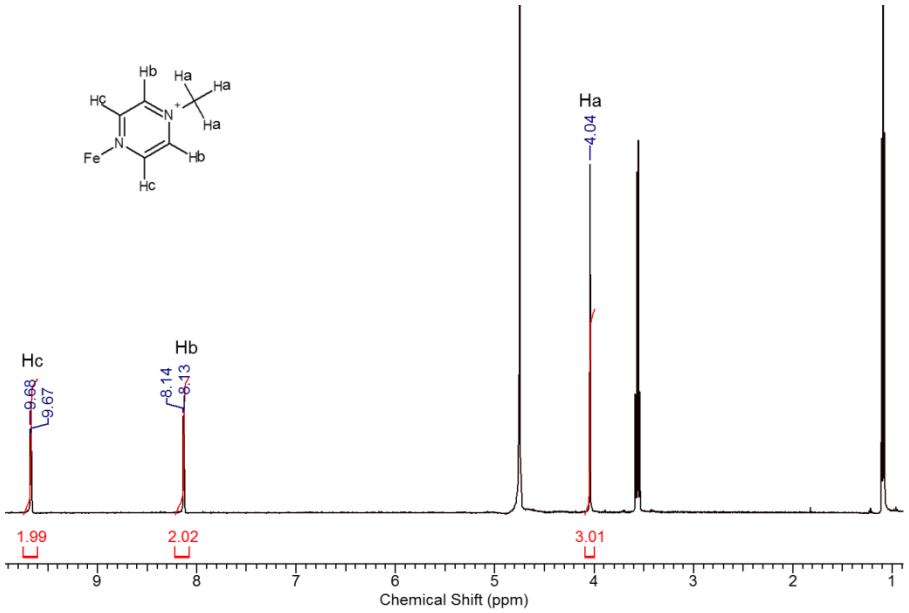

Figure 20. ^{1}H NMR spectrum of PCF-mpz in D_2O. At 3.61 and 1.14 ppm are peaks from ethanol.

4.2.2. Electronic Spectroscopy

The electronic structure of the complex was confirmed by electronic spectroscopy (**Figure 21**). The molar absorption coefficient (ε) of precursor and the complex was calculated using the Beer-Lambert law (**Equation 15**):

$$A = \varepsilon \, l \, c \qquad (\mathbf{15})$$

where A is the absorbance (a.u.), l is the optical path length (cm) and c is the concentration of the solution (mol L^{-1}).

PCF-amin shows a weak band at 402 nm (ε = 4.26 x 10^2 L mol^{-1} cm^{-1}) that is assigned to a ligand field transition[9]. When ammonia is replaced by mpz a strong band appears in the visible region of the spectrum. The strong absorption means that a charge transfer occurs. Then, at 661 nm (ε = 7.43 x 10^3 L mol^{-1} cm^{-1}) a metal-to-ligand charge transfer (MLCT) Fe(dπ)→mpz(pπ*) is observed. This transition is responsible for the blue color of complex[2]. A weak band at 382 nm also appears in the complex spectrum and can be assigned to a d-d transition (ligand field transition – LFT).

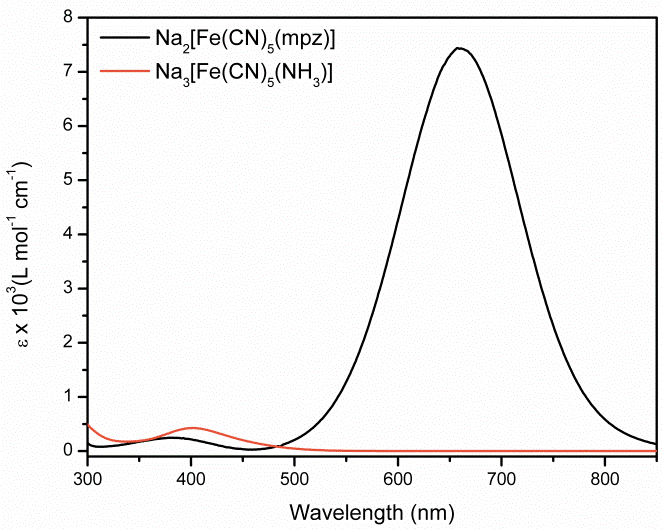

Figure 21. Molar absorption coefficient in function of wavelength of PCF-amin and PCF-mpz in water.

The complete spectrum of the PCF-mpz is demonstrated below (**Figure 22**). The intra ligand transition (IL) of mpz is observed (277 nm) with practically the same wavelength when it is a free ligand (274 nm), as reported[3a]. At 220 nm a MLCT between the cyanide ligands and iron(II) is observed. The intra ligand transition of the cyanide has higher energy and the band is at lower wavelengths (not shown). The relation between the molecular orbital energy and the respective transitions is presented in **Figure 22**[106].

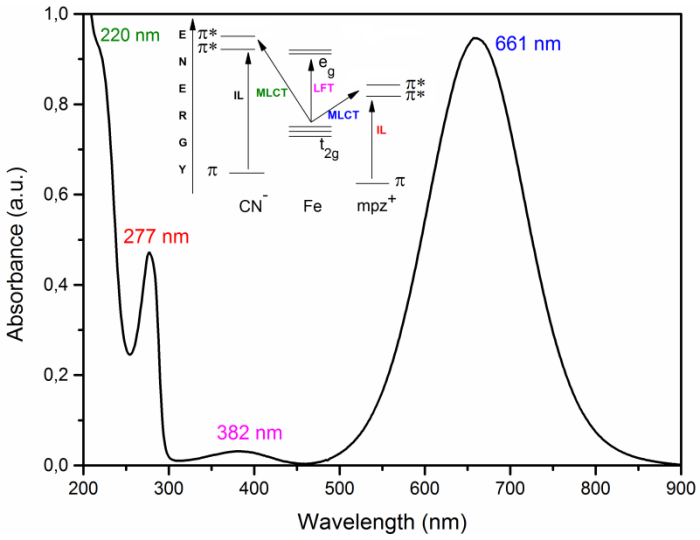

Figure 22. UV-Vis spectrum of PCF-mpz.

4.2.3. Vibrational Spectroscopy

In order to verify the coordination mode of the ligand, the well-known infrared spectrum of PCF-amin was obtained to compare with PCF-mpz (**Figure 23**) and the observed values are showed in **Table 3**.

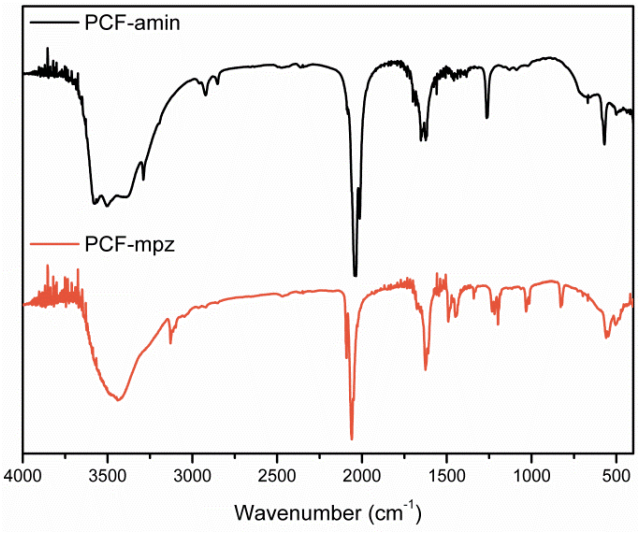

Figure 23. Infrared spectra of PCF-amin and PCF-mpz.

Table 3. Observed infrared bands of PCF-amin and PCF-mpz[9, 97].

Wavenumber (cm^{-1})		**Assignment**
$Na_3[Fe(CN)_5(NH_3)]$	$Na_2[Fe(CN)_5(mpz)]$	
-	3128	$\upsilon(CH + CH_3)$
3288, 2922, 2851	-	$\upsilon(NH_3)$
2039	2060	$\upsilon(CN)_{cis}$
2014	2091	$\upsilon(CN)_{trans}$
1652	-	$\delta_d(NH_3)$
-	1625, 1609	$\upsilon(CN_{ring})$
1264	-	$\delta_s(NH_3)$
-	1198	ring deformation
570	560	$\delta_d(Fe\text{-}CN)_{cis}$
584	546	$\delta_d(Fe\text{-}CN)_{trans}$

υ – stretching; δ – deformation.

These results indicate that PCF-mpz presents characteristic bands of pyrazinic ring (1198 cm^{-1}) and methyl group (3128 cm^{-1}), from pyrazinium. Moreover, strong vibrational modes of cyanide group and of Fe-CN are present in the spectrum. No vibrational modes of the precursor are present in infrared spectrum of PCF-mpz, which indicates that complex was obtained.

Focusing on the stretching of Fe-CN and CΞN some differences are observed. First, $\delta_d(Fe\text{-}CN)_{cis}$ has higher wavenumber in PCF-amin than in PCF-mpz. In addition, $\delta_d(Fe\text{-}CN)_{trans}$ of PCF-amin shifts to lower wavenumbers while in PCF-mpz, it shifts to a higher wavenumber. Due to the presence of the ligand in the complex structure, Fe-CN *trans* to it has a different stretching energy. When the ligand is NH_3, it influences the electronic density from the metal, with a small σ contribution. This allows the bond to be shorter $Fe\text{-}CN_{trans}$ (584 cm^{-1}). Changing the ligand to mpz implies in an electron density contribution from metal to the ligand that increases the distance of $Fe\text{-}CN_{trans}$ (546 cm^{-1}). Observing $Fe\text{-}CN_{cis}$ it is possible to describe total of four CN^- mutually contributing with same electron density (beyond $Fe\text{-}CN_{trans}$ contribution), weakening their coordination. Clearly, this participation of $Fe\text{-}CN_{trans}$ is more accentuated for NH_3 (570 cm^{-1}) when compared to mpz (560 cm^{-1})[24, 27].

Second, for υ(CN), the inverse is observed. This fact is closely related to the Fe-CN bond. The more electron density at metal center, the greater is the distance between Fe and CN^- and the stronger will be CΞN bond[107].

4.2.4. Cyclic Voltammetry

Cyclic voltammetry was used for the electrochemical characterization of the complexes. Pentacyanidoferrates(II) show a well-defined electrochemical process that is influenced by the nature of the ligands. The obtained voltammograms for the $[Fe(CN)_5(NH_3)]^{3-}$ and for the $[Fe(CN)_5(mpz)]^{2-}$ are shown in **Figure 24**.

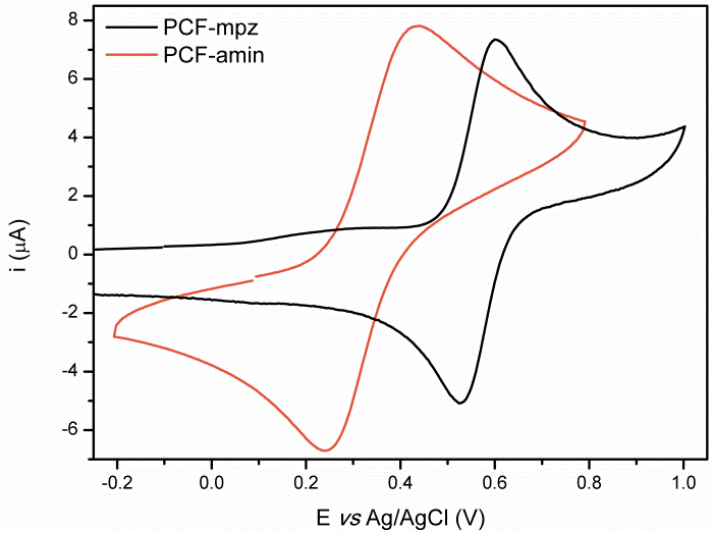

Figure 24. Voltammograms of the aqueous solutions of PCF-amin and PCF-mpz at scan rate of 100 mV s^{-1} (supporting electrolyte KCl 0.1 mol L^{-1}).

The voltammograms show a redox process at E°' = 0.56 V *vs* Ag/AgCl, which has been assigned to the $[Fe(CN)_5(mpz)]^{2-/3-}$ couple. All the measured potentials are consistent with the values reported in the literature[3a, 9]. The difference between the cathodic and anodic peaks indicates that the redox process exhibits quasi-reversible behavior (ΔEp = 81 mV at scan rate of 25 mV s^{-1}, see **Table 4**).

The variation of the half-wave potential has confirmed that a substitution of the ligand NH_3 by mpz has occurred. These potentials allow evaluating the electronic nature of each ligand. The voltammograms show an increase from 0.34 to 0.56 V *vs* Ag/AgCl, due to the change of the ligands, NH_3 to mpz[24], respectively. This increase reflects the greater electronic density removal due to the coordination of N-heterocyclic ligand, when compared with NH_3, resulting in a more difficult oxidation of iron[6, 36].

Figure 25 (left) shows the cyclic voltammograms of a solution of the PCF-mpz, with KCl 0.1 mol L^{-1}. The obtained parameters are shown in **Table 4**. The redox current peaks, and consequently the $E_{1/2}$ and ΔE, do not change with the scan rate, a characteristic of reversible process. However, the ratio between the cathodic and anodic current peaks (i_{ap}/i_{cp}) is distant from unit in all scan rates. It can be explained due to the oxidized form of PCF-mpz that change the ligand by water slowly, without any apparent changes in the measured potential[6], but with a decrease in the cathodic current. Another point that needs

to be discussed is about the ΔE. It is expected for this complex to be 60-65 mV, but ΔE = 81 mV was obtained. This increase of the separation in potential peaks indicates a decrease in the heterogeneous electron-transfer rate (HET). If the surface is covered by a monolayer of nonspecific and non-electroactive absorbers, HET decreases, showing a problem in the control of the surface composition when the glassy carbon electrode is polished[108]. Finally, there is a regular variation of the current peaks with $v^{1/2}$ (**Figure 25**, right), indicating a mass transfer process controlled by diffusion at slow scan rates (**Equation 16**).

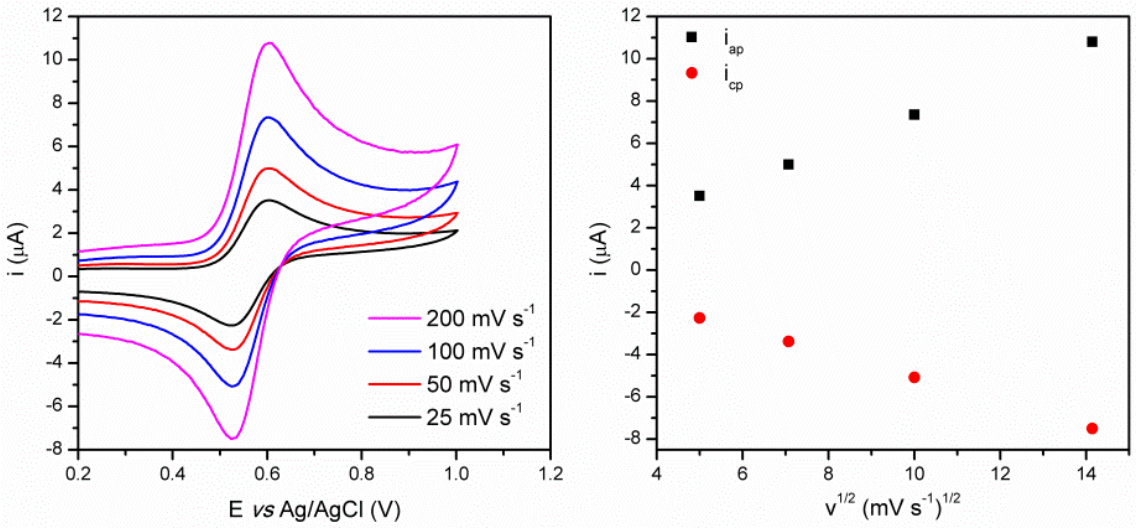

Figure 25. Voltammograms of the aqueous solution of PCF-mpz in different scan rates (left); relation of current peak and scan rates (right). Supporting electrolyte KCl 0.1 mol L^{-1}.

Table 4. Calculated electrochemical parameters of PCF-mpz.

v (mV s^{-1})	E_{ap} (V)	E_{cp} (V)	$E_{1/2}$ (V)	ΔEp (mV)	I_{ap} (μA)	I_{cp} (μA)	I_{ap}/i_{cp}
25	0.605	0.524	0.564	80	3.51	-2.27	1.55
50	0.605	0.524	0.564	80	4.99	-3.38	1.48
100	0.600	0.524	0.562	80	7.35	-5.08	1.45
200	0.605	0.524	0.564	80	10.8	-7.50	1.44

In order to use the Randles-Sevcik equation (**Equation 16**) the diffusion coefficient from PCF-mpz can be calculated.

$$i_p = 2{,}69 \times 10^5 \, n^{3/2} \, A \, D^{1/2} \, C \, v^{1/2} \qquad (\mathbf{16})$$

where i_p is the peak current, n is the number of electrons involved in the redox process, A is the electrode area, D is diffusion coefficient of the electroactive specie, C is the concentration of the solution and v is the scan rate.

Since the number of the electrons involved in the redox process, the electrode area (4.62×10^{-2} cm^2) and the concentration of PCF-mpz solution (5.0×10^{-3} mol L^{-1}) are known, the diffusion coefficient was obtained (1.28×10^{-6} cm^2 s^{-1}). This result means that PCF-mpz diffuses through the solution about five-fold slower than HCF (6.67×10^{-6} cm^2 s^{-1})[109].

Moreover, for comparison, **Figure 26** presents the voltammograms of mpz and PCF-mpz. It can be seen that the reduction process of mpz ($E_{1/2} \cong$ -0.82 V *vs* Ag/AgCl), shifts to more negative potentials. This implies an increase of energy to reduce mpz when it is coordinated, due to the back-donation of the N-heterocyclic group. Also, the coordination improved the reversibility of mpz/mpz• redox process[16]. The redox process of the iron can mask other signals of the ligand appearing near this value. A signal at 0.274 V *vs* Ag/AgCl appears when the scan rate increased, but there is no record of it in the literature.

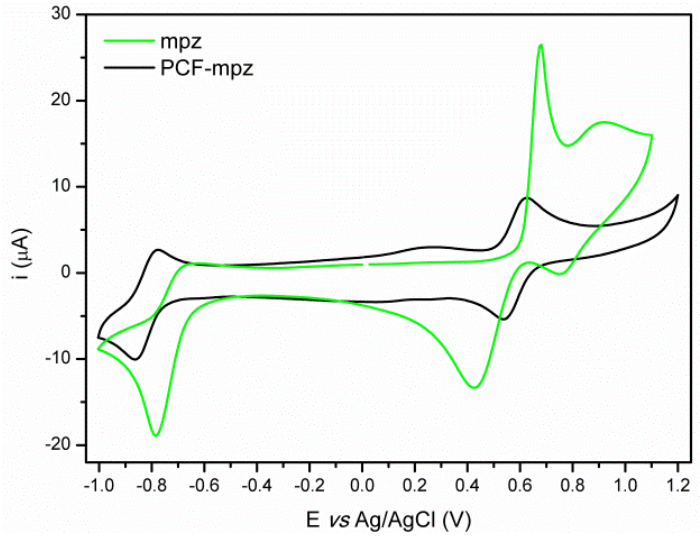

Figure 26. Voltammograms of the aqueous solutions of PCF-mpz and of mpz at scan rate of 100 mV s^{-1} (supporting electrolyte KCl 0.1 mol L^{-1}).

4.2.5. Stability and reactivity of PCF-mpz

4.2.5.1. Electrochemical behavior of PCF-mpz solution at different pH

A study of the electrochemical behavior of PCF-mpz at pHs 2-11 was performed at 0.4 to 0.8 V *vs* Ag/AgCl potential range and scan rate of 100 mV s^{-1} (**Figure 27**). In this potential range PB-mpz formation was not observed. The redox pair of $[Fe(CN_5)(mpz)]^{2-/3-}$ showed a quasi-reversible behavior at low pH values.

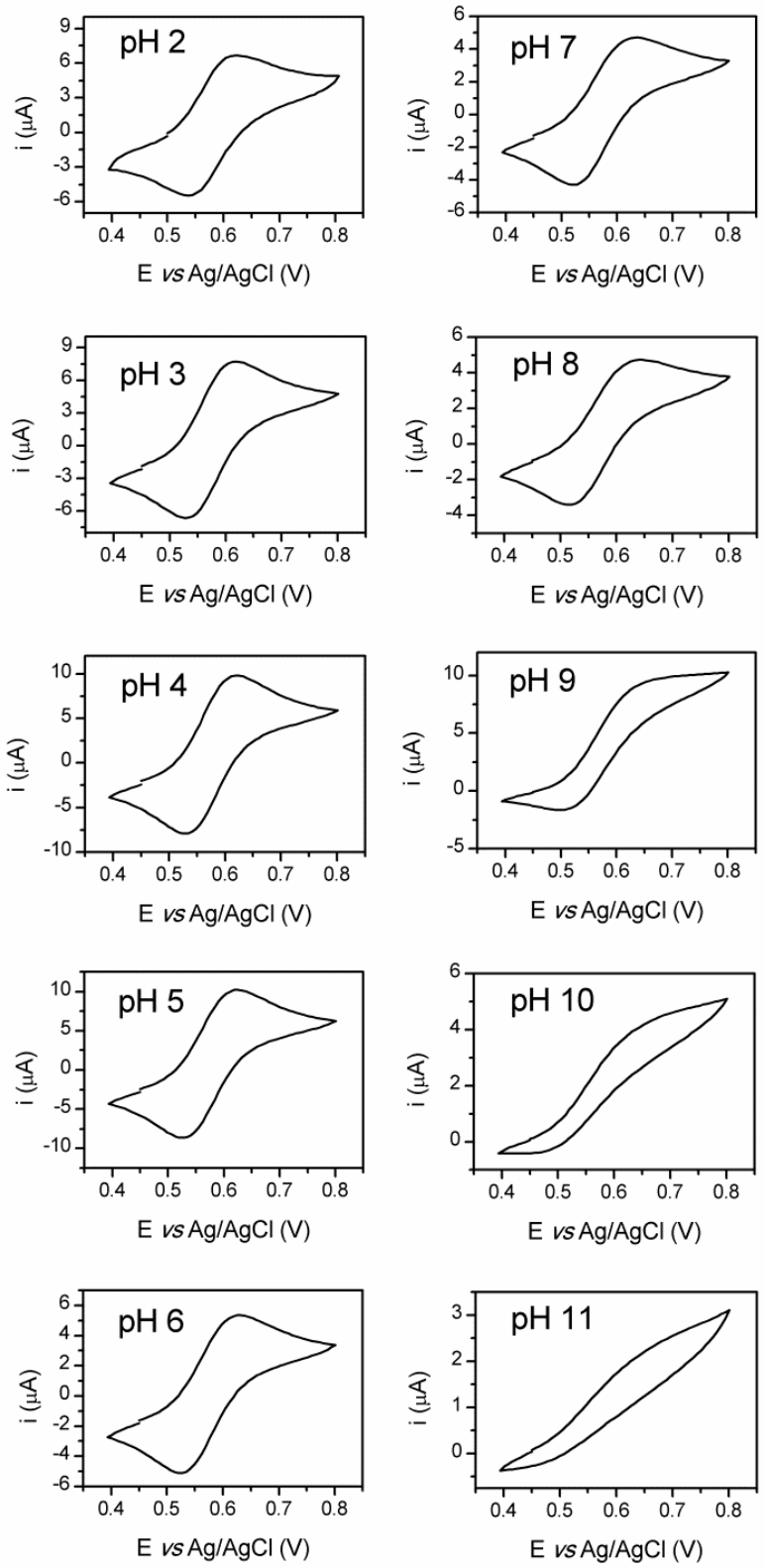

Figure 27. Electrochemical behavior of PCF-mpz at pH 2-11 at scan rate of 100 mV s^{-1} (supporting electrolyte KCl 0.1 mol L^{-1}).

Figure 28a presents the relation between ΔE and pH obtained from voltammograms. With the increase of pH, the processes become more

irreversible and E_{ap} shifts to potentials more positive than 0.8 V, indicating that PCF-mpz is not stable in alkaline solutions. Thus, **Figure 28a** and **Figure 28b** are in function of pH 2-8 range.

These observations suggest that some species can be formed and they have different diffusion coefficients that affect the shape of the voltammograms. Formation of polynuclear complexes or FeOOH could occur[9, 110].

Figure 28b evaluates E_{ap} as a function of pH. The results show lower potentials occuring at pH 3.0 and 4.0 (0.618 V). However, in aqueous solutions, the anodic peak potential is at 0.600 V, meaning that it is easier to oxidize iron(II) in water than in buffer solutions (ΔE is smaller in water than buffer solution, as well), designating a different electronic transfer that depends on the medium.

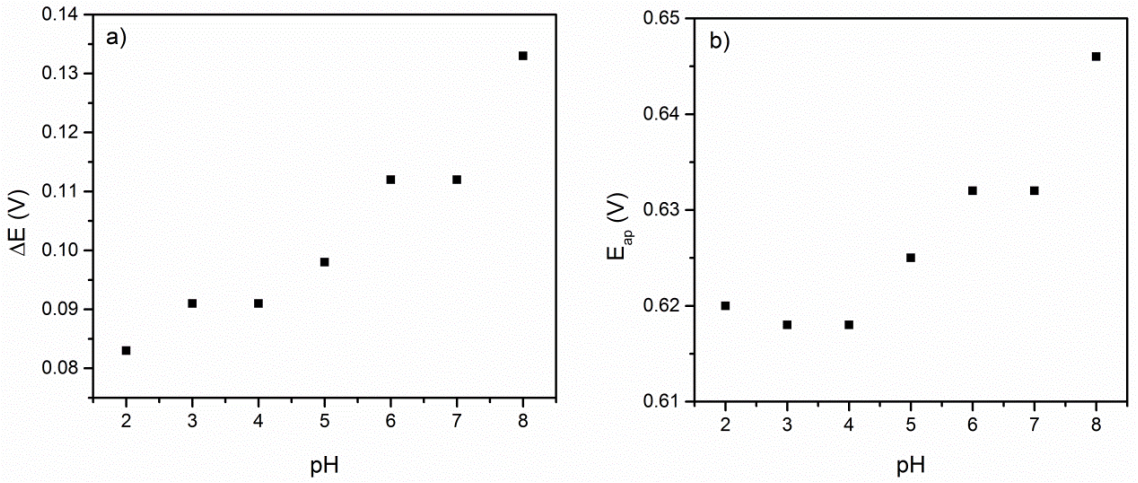

Figure 28. Relation of potential parameters and pH at 0.4 to 0.8 V *vs* Ag/AgCl range and scan rate of 100 mV s^{-1}. (a) Difference between peak potentials *vs* pH. (b) Anodic peak potential vs pH.

4.2.5.2. The stability of the complex in different pH

Using UV-Vis spectroscopy, a study about the influence of the pH in the complex stability was performed. At pH 2.0 a hypsochromic shift of the MLCT band is observed, in comparison with neutral solutions, with the maximum absorption wavelength changing to 652 nm (**Figure 29**). This corresponds to a

protonation of cyanide ligands, which stabilizes the d_π orbitals, decreasing the electronic density of the metal[41].

At acidic pH the aquapentacyanidoferrate(II) decomposes into Fe^{II} which, in aqueous solution, is oxidized to Fe^{III}. Thus, these ions can interact with the cyanidoferrates(II) to form PB, but in the case of mpz the process is too slow. To verify PB-mpz formation, the complex of this work was added to an acid solution and the complete formation of the compound was observed only after 2 weeks what is interesting because other pentacyanidoferrate(II) complexes can produce PB immediately or after short periods of time[8-9].

At alkaline pH the dissociation was also observed. At high pH, there is a strong competition between CN^- and OH^- for Fe. Mixed complexes can be formed and there is a possibility of the precipitation of FeOOH. Even the stable complex $[Fe(CN)_6]^{3-}$ can undergo substitution reactions at higher pH values. At pH 9.0 and 10.0 no significant variation of the MLCT was observed, probably due to the formation of others species cited above[9].

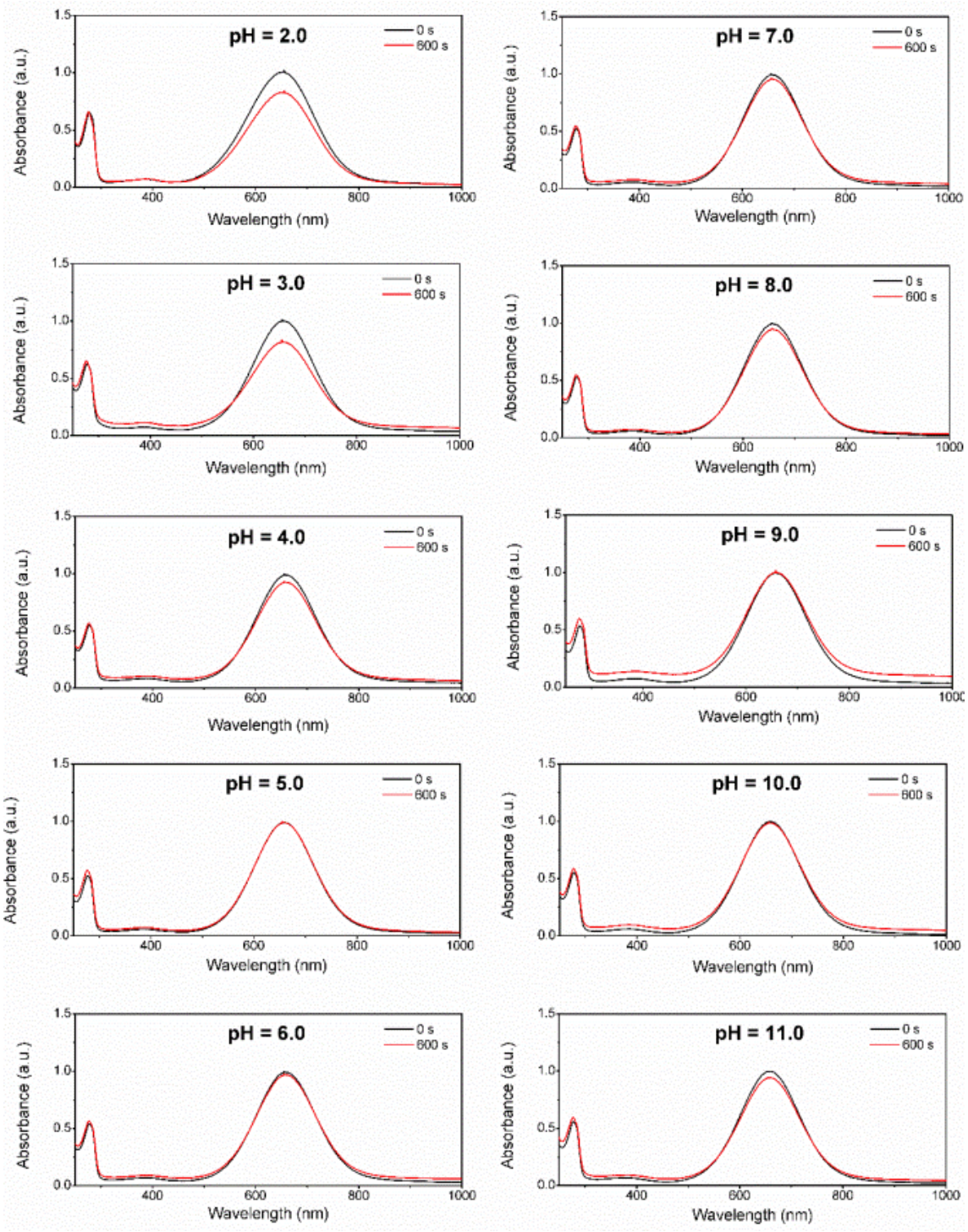

Figure 29. UV-Vis Spectra of PCF-mpz in buffer solutions among pH 2.0 to 11.0.

4.2.5.3. Substitution kinetics of the ligand in the presence of DMSO

The replacement of the ligand mpz by DMSO was investigated, using aqueous solutions of complex with an excess of DMSO. It is reported that coordinated mpz is inert[3a], but it is important to understand this inertia for

ligand exchange for further comparison with PB-mpz. Moreover, N-heterocycles ligands coordinated to pentacyanidoferrate(II) are known to undergo substitution by DMSO[3b]. In this complex, the coordination is by sulphur atom of DMSO and it doesn't have a charge transfer band on the UV-Visible region. The substitution kinetics can be monitored by the decrease of the absorbance of MLCT band of PCF-mpz (**Figure 30a**).

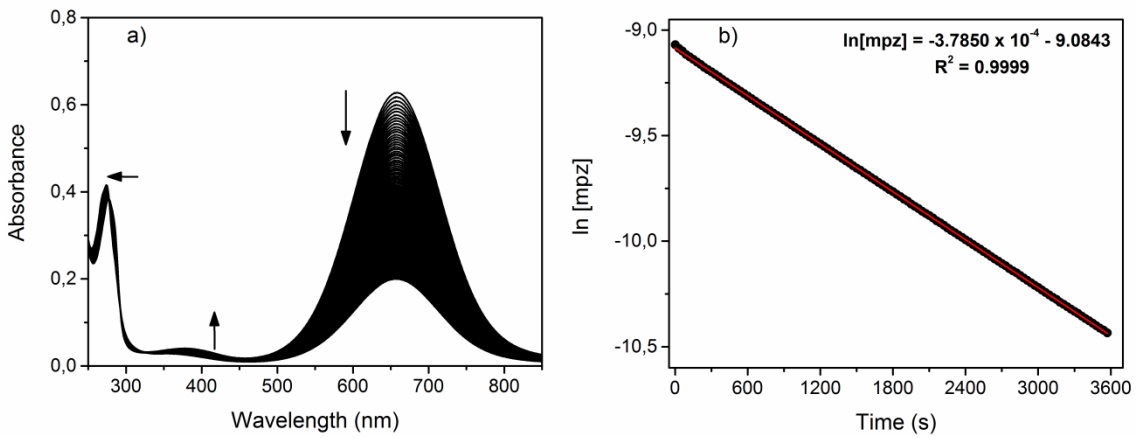

Figure 30. (a) Electronic spectrum of PCF-mpz and DMSO solution. (b) Linear relation of ln [mpz] and time.

Figure 30a shows not only a decrease of the MLCT, but also a shift in the mpz transition [decreasing at 277 (from PCF-mpz) nm and increasing at 274 nm (from free mpz)] and the increase to an absorption peak centered at 352 nm, characteristic of DMSO coordinated to PCF[111].

The mechanism of the substitution of ligand in pentacyanidoferrate(II) was studied already and it can be rationalized by dissociative mechanism described by **Equations 17**, **18** and **19**. In the complex $[Fe(CN)_5L]^{n-}$, the rate constant for substitution of ligand L is independent of L', although the substitution rate varies with different ligands.

$$[Fe(CN)_5L]^{(3-n)-} \underset{k_L}{\overset{k_{-L}}{\rightleftharpoons}} [Fe(CN)_5]^{3-} + L^n \quad (\mathbf{17})$$

$$[Fe(CN)_5]^{3-} + H_2O \underset{k_{-w}}{\overset{k_w}{\rightleftharpoons}} [Fe(CN)_5(H_2O)]^{3-} \quad (\mathbf{18})$$

$$[Fe(CN)_5]^{3-} + L'^{n'} \underset{k_{-L'}}{\overset{k_{L'}}{\rightleftharpoons}} [Fe(CN)_5L']^{(3-n')-} \quad (\mathbf{19})$$

It is assumed that when both L and L' are stronger nucleophiles than water, aquapentacyanido formed (**Equation 19**) is in insignificant concentrations and has no effect on the mechanism. In this study, L = mpz and L' = DMSO. Therefore, it is possible to obtain the K_{obs} by the **Equation 20** below:

$$K_{obs} = \frac{K_{-mpz} K_{DMSO}\,[DMSO]}{K_{mpz}[mpz] + K_{DMSO}\,[DMSO]} \quad (\mathbf{20})$$

Using excess of DMSO to obtain pseudo-first-order conditions, it can be considered that $K_{DMSO}[DMSO] >> K_{mpz}[mpz]$ and the observed rate constant is equal to the dissociation rate constant of the mpz ligand (K_{-mpz}), given by **Figure 30b** and **Equation 21**.

$$K_{obs} = K_{-mpz} \quad (\mathbf{21})$$

The found rate constant was 3.78 x 10^{-4} s^{-1}, similar with described in reference (2.80 x 10^{-4} s^{-1})[4].

4.3. Ferric pentacyanido(N-methylpyrazinium)ferrate(II) – PB-mpz

In order to characterize and evaluate the performance of the PB-mpz, most of the experiments were also performed with the traditional Prussian blue, for comparison purposes, and they are discussed in the next topics.

Considering that there are two types of iron species in this structure coordinated with different atoms, they need to be distinguished. For this reason, they will be called $Fe_{(c)}$ and $Fe_{(N)}$, meaning iron coordinated to carbon and iron coordinated to nitrogen, respectively.

4.3.1. Electronic Spectroscopy

Analyzing the spectra of the PCF-mpz, PB-mpz, and PB (**Figure 31**) the transitions for the latter were proposed. PCF-mpz transitions were described at

item **4.2.2** and PB transitions are summarized in **Table 5**. Data were also normalized for the purpose of comparison between spectra.

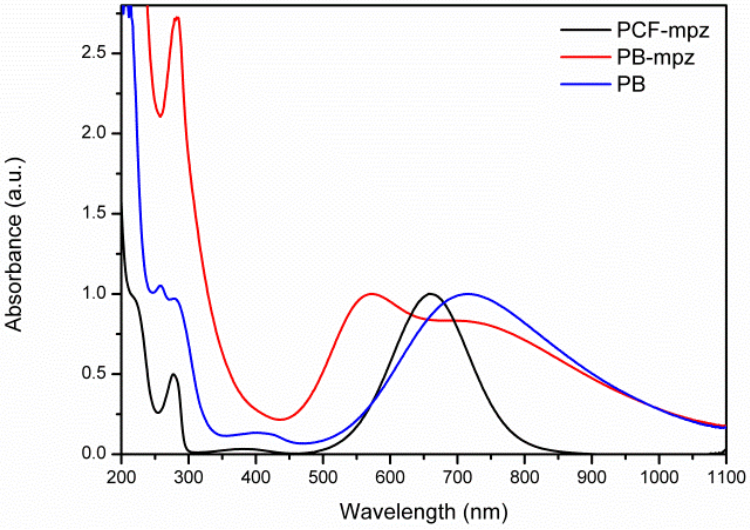

Figure 31. UV-Visible spectra of cyanidoferrates.

Table 5. Maximum wavelength of cyanidoferrates' transitions.

Complex/Transition	IL	LMCT	LFT	MLCT	IT
PCF-mpz	277 nm	-	382 nm	220 nm 661 nm	-
PB	-	258 nm 278 nm	-	220 nm	401 nm 717 nm
PB-mpz	282 nm	#	-	220 nm 573 nm	#' 708 nm

IL – intra ligand; LMCT – ligand-to-metal charge transfer; LFT – ligand field transition; MLCT – metal-to-ligand charge transfer; IT – intervalence transition. The symbols # and #' are to indicate that the bands may be masked by the others absorptions.

The strong absorptions at 220 nm are assigned to MLCT Fe(dπ) → CN(pπ*), like in PB. Intra ligand transfer occurs at 282 nm, with a red shift compared to PCF-mpz. With the coordination of Fe^{III} to the nitrogen from CN group of PCF-mpz, two bands in the visible region are expected: a MLCT Fe(dπ) → mpz(pπ*), that has an increase in energy, with a maximum at 573 nm,

responsible to the color of PB-mpz; and an intervalence transition (IT), Fe^{II}-CN-Fe^{III}, like in PB, at 708 nm. LMCT CN(pπ) → Fe^{III}(dπ) and another IT may be masked by others absorptions in the same regions.

To prove the theory about these transitions, spectroelectrochemistry was done. But, before the discussion about this technique, it is important to take a look in to the behavior of the cyclic voltammogram of PB-mpz.

4.3.2. Cyclic Voltammetry

Cyclic voltammetry was used to study the electrochemical behavior of PB-mpz. Thus, after immobilization of the compound, the potential was scanned from -1.2 to 1.2 V *vs* Ag/AgCl in aqueous solution of KCl 0.1 mol L^{-1} and scan rate of 100 mV s^{-1}. PB was subjected to an identical process, with a smaller potential range (from 0.2 to 1.2 V), due to no redox processes in the negative side of the voltammogram. PCF-mpz is represented for comparison (**Figure 32**). The electrochemical parameters are shown in **Table 6**.

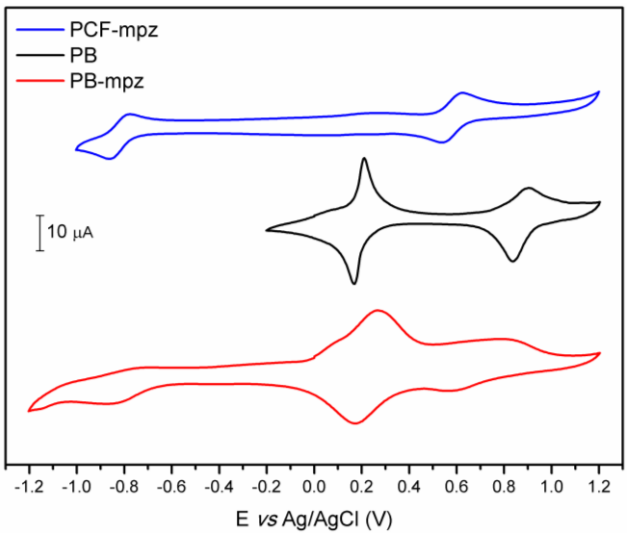

Figure 32. Voltammograms of PCF-mpz solution and PB and PB-mpz films at scan rate of 100 mV s^{-1} (supporting electrolyte KCl 0.1 mol L^{-1}).

Table 6. Electrochemical parameters of cyanidoferrates at scan rate of 100 mV s^{-1} in aqueous solution of KCl 0.1 mol L^{-1}.

		PCF-mpz	PB	PB-mpz
R1	E_{ap} (V)	-0.772	-	-0.690
	E_{cp} (V)	-0.863	-	-0.876
	$E_{1/2}$ (V)	**-0.818**	-	**-0.783**
	ΔEp (V)	**0.091**	-	**0.186**
O1	E_{ap} (V)	0.600	0.211	0.267
	E_{cp} (V)	0.524	0.181	0.171
	$E_{1/2}$ (V)	**0.562**	**0.196**	**0.219**
	ΔEp (V)	**0.076**	**0.030**	**0.096**
O2	E_{ap} (V)	-	0.906	0.790
	E_{cp} (V)	-	0.836	0.564
	$E_{1/2}$ (V)	**-**	**0.871**	**0.677**
	ΔEp (V)	**-**	**0.070**	**0.226**

The reduction process of mpz (R1) can be seen at negative potentials. In this compound mpz• looks unstable, similar to free mpz voltammogram (**Figure 15**), but with an intermediate $E_{1/2}$ if compared to PCF-mpz and mpz ($E_{1/2}$ = -0.706 V). This observation shows that mpz is on the structure. At negative potentials, PB and PB-mpz are in the reduced form (Prussian White – PW and PW-mpz, respectively).

Shifting to positive potentials, PW and PW-mpz starts to oxidize to PB and PB-mpz, respectively. In PB, all the coordinating groups are CN^- and they contribute equally with σ-donation and π-reception. CN^- is a good π-aceptor, but also a great σ-donor[24]. Consequently, an increase in the charge density on $Fe_{(N)}$ facilitates the oxidation of this metal ($E_{1/2}$ = 0.196 V). For PB-mpz, due to the presence of mpz in the structure, some sites of $Fe_{(N)}$ are disabled to coordination with cyanide groups and they can be occupied by solvent (water). Since water has smaller σ-donor character than CN^-, $Fe_{(N)}$ has smaller charge density than in PB. Thus, a small shift at the potential is observed ($E_{1/2}$ = 0.219

V). Another point that needs to be discussed is about the width of the redox wave. It is much larger than the wave potential of PB, with an addition of a shoulder that appears at 0.1 V. These factors indicate different coordination by the $Fe_{(N)}$ and the shoulder can be assigned to few $Fe_{(N)}$ coordinated with six CN^-, like in PB (i.e. there is a variation in the number of H_2O and cyanide coordinated, where a total of six CN^- gives a lower potential). Also, these observations justify the increase in the ΔE. The full width at half-height (FWH) of PB-mpz was found to be 226.6 and 216.5 mV for the anodic and cathodic processes, respectively (60.4 and 65.5 mV to PB process). These values are different from the theoretical (90.6/n mV) and may arise from lateral interactions, inhomogeneity of surface sites and ion interactions[112], as well as evidence of the presence of overlapping of multiple peaks[8]. A specific topic about the proportion of PCF-mpz:Fe^{III} has been discussed (see section **4.3.5**).

Increasing the potential, part of iron(II) starts to oxidize and the Berlin Green (BG, BG-mpz to the cyanidoferrate in study) is formed. Thus, PB has an oxidation potential more positive than PB-mpz. This can be explained by the lack of cyanide bridge caused by the presence of mpz. In PB, the presence of $Fe^{III}_{(N)}$ decreases the charge density, increasing the bond distance of Fe^{II}-CN. This fact stabilizes $Fe_{(C)}$ due to the lowering in energy of t_{2g} orbitals, increasing the oxidation potential (0.871 V). In the case of PB-mpz, the same is expected, but there is a lower amount of cyanide bridges. Therefore, the CN bridge has more contribution to the stabilization of metal than CN^- that is not bridged (and more than mpz, also). Consequently, the charge density on $Fe_{(C)}$ is greater in PB-mpz than in PB, increasing the energy of d orbitals and decreasing the oxidation potential (0.677 V).

4.3.3. Spectroelectrochemistry

Based on the electrochemical behavior and taking into account the transitions assigned previously (**Table 5**) a spectroelectrochemical experiment was performed in order to confirm the assignments. The spectra can be seen in **Figure 33**.

Firstly, the reduced form of PB-mpz was studied. Iron of PCF-mpz in the structure maintains the oxidation state and only Fe(III) was reduced. Shifting to more negative potentials (-1.0 V) Fe^{II}/Fe^{II} state was obtained and no transition between irons occurs. This means that the intervalence band disappears, as expected. Also, the band initially at 573 nm shifts to 625 nm (from -0.65 V). With the reduction (Fe^{III}-NC to Fe^{II}-NC) there is an increase of negative charge in the compound. This contributes to a rise in the energy from d orbitals of iron coordinated with mpz. Consequently, the MLCT has a red shift[8]. Finally, the band at UV region has its intensity lowered and it can be proved that it is from mpz. To compare this transition, spectroelectrochemistry studies of mpz were performed (**Figure 32**, insert).

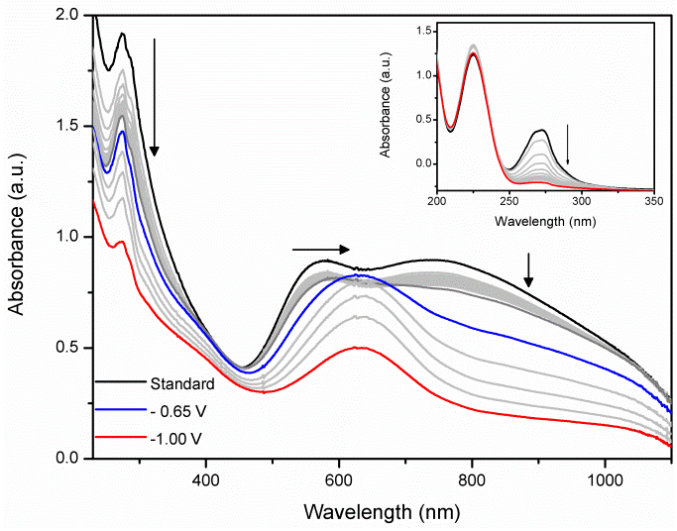

Figure 33. PB-mpz spectrum in aqueous solution (KCl 0.1 mol L^{-1}). Insert: mpz spectrum. The data was taken by applying potentials range from 0 to -1.0 V *vs* Ag/AgCl. Work electrode platinum, reference electrode calomel and counter electrode platinum wire.

Then, the assignment of PB-mpz transitions (see section **4.3.1**) are in agreement with this technique. Besides being able to justify the transitions in the visible region, it was possible to confirm the transition of mpz in the ultraviolet region.

4.3.4. Vibrational Spectroscopy

Vibrational energies vary between chemical bonds. Thus, vibrational spectroscopy on the infrared region (IR) can be a powerful technique to prove the difference of PB to PB-mpz.

The data collected for both are represented in **Figure 34** and the assignments are described in **Table 7**. Assignments of PCF-mpz are summarized, for comparison.

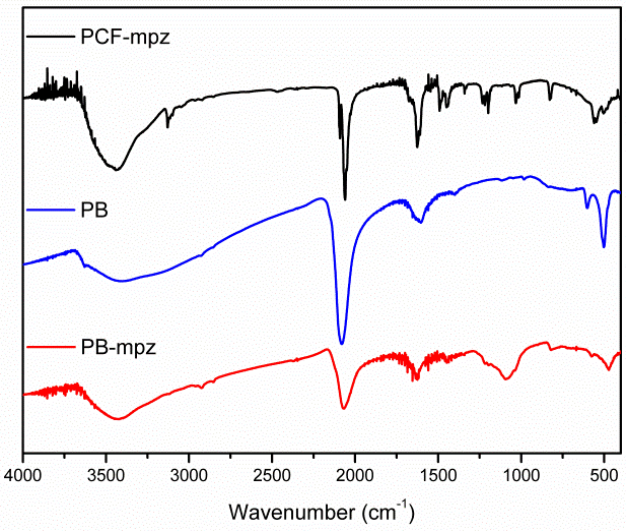

Figure 34. IR spectra of PCF-mpz, PB and PB-mpz.

Table 7. Observed infrared bands of PCF-mpz, PB and PB-mpz[113].

Wavenumber (cm^{-1})			Assignment
PCF-mpz	PB	PB-mpz	
3431	3402	3433	υ(OH)
2091^{t}, 2060^{c}	2080	2070	υ(CN)
1625’	1602	1623	δ(H-O-H)
1194	-	1093	ring deformation
560^{c}*, 546^{t}*	600, 502	573, 472	$\delta(Fe^{II}\text{-}CN\text{-}Fe^{III})$

υ – stretching; δ – deformation. (t) – $\upsilon(CN)_{trans}$; (c) – $\upsilon(CN)_{cis}$; (*) – for PCF-mpz the assignment is δd(Fe-CN); (‘) – there is another vibration, υ(CNring), in this wavenumber, also.

The presence of a ring deformation from PCF-mpz in PB-mpz can be observed (1093 cm^{-1}), and also a υ(CN), at 2070 cm^{-1} and $\delta(Fe^{II}\text{-}CN\text{-}Fe^{III})$, at 573 and 472 cm^{-1}. These informations can indicate formation of complex.

The frequencies order of υ(CN) is PB > PB-mpz > PCF-mpz (cis) and can be explained. Generally, an increase in the υ(CN) mode is observed in shifting from terminal cyanide ligands to linear bridging, like Fe-CN-Fe[107]. PB has more cyanide bridges than PB-mpz (see next section for more details) and PCF-mpz has no cyanide bridges. Moreover, the band related to this stretch in PB and PB-mpz is wider, meaning that there are many types of cyanides in their structures. The presence of water is due to it coordinated and the hydrated one.

4.3.5. Determination of composition of PB and PB-mpz – Job's Method

The main question of this work involves an analysis on the structure of PB-mpz and some evidences about the presence of the ligand on the structure were observed. A single-crystal of this compound or computational calculations might support some discussions. However, until now only the structure of PCF-mpz was solved[27]. On the other hand, a simpler way to collect some indication of the structure, but with great limitations, is by applying Job's method[114].

Job's method is carried out by mixing aliquots of two equimolar solutions of metal and ligand. It is essential to keep the total analytical concentration of reactants constant, varying only the ligand:metal ratio (**Equation 22**).

$$C_M + C_L = k \qquad (\mathbf{22})$$

where C_M and C_L are the analytical concentrations of metal and ligand, respectively, and k is a constant. The corrected absorbance (Y) is plotted as a function of molar fraction of ligand or metal. The resulting curves yield a maximum indicating the ligand:metal ratio of the complex in solution. The corrected absorbance is defined by **Equation 23**:

$$Y = A - (\varepsilon_M C_M + \varepsilon_L C_L)b \qquad (\mathbf{23})$$

where A is the measured absorbance, ε_M and ε_L are the absorptivities of metal and ligand, respectively, and b is the optical path length. Also, it is important to keep in mind that the molar fraction (**Equation 24**) in this context is not the true molar fraction (solvent is omitted from its calculation).

$$X_M = \frac{C_M}{C_L + C_M} \quad (\mathbf{24})$$

The molar fraction of ligand is similarly defined[114a].

According to the description above, Job's method was used to give some idea about the ratio of hexacyanidoferrate(II):Fe^{III} (to PB) and PCF-mpz:Fe^{III} (to PB-mpz). In order to perform this, a region in the spectrum that has predominance of intervalence band was chosen. Thus, it is possible to know the proportion of cyanide bridge formed and, consequently, the stoichiometry of PB and PB-mpz. For PB, the absorbance was collected at 710 nm. Hexacyanidoferrate(II) (HCF) and ferric chloride do not exhibit any transition in the visible spectrum and the value of the correct absorbance is equal to measured absorbance. For PB-mpz, due to the intense MLCT band from PCF-mpz being between MLCT and IT wavelength from PB-mpz (**Figure 31**), the chosen wavelength for this experiment was at 850 nm, where a small portion of MLCT can be overlapped. Then, Y was calculated. **Figure 35** shows Y versus $X_{Complex}$ plot, where complex means HCF, to PB, and PCF-mpz, to PB-mpz.

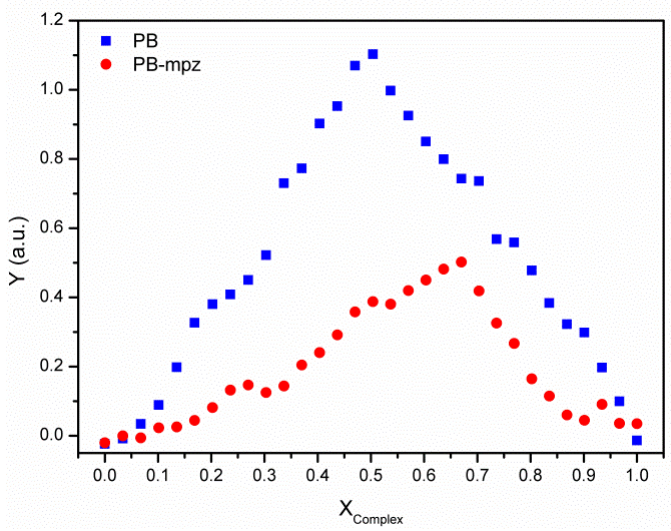

Figure 35. Job's plot obtained from intervalence transition of ferric cyanidoferrate(II) (710 nm to PB and 850 nm to PB-mpz). $X_{Complex}$ = HCF, to PB and PCF, to PB-mpz.

Important information can be taken from this data. Firstly, considering the Beer's law (**Equation 15**), the maximum of the curves means a higher concentration of the product. Also, it's possible to see some lower curves in both cases. This indicates that subproducts are formed in different ratios. PB exhibited a broad maximum at X_{HCF} = 0.5, indicating the formation of a 1:1 HCF:Fe^{III} under these experimental conditions. For PB-mpz, when $X_{PCF\text{-}mpz}$ = 0.5 the formation of PB-mpz shows a maximum, but with the increase in the proportion of PCF-mpz, the intensity decreases. Though the proportion is not 1:1, because one site is coordinated with mpz, then the number of coordinated iron(II) is higher than $X_{PCF\text{-}mpz}$ = 0.55 ratio. Continuing with an increase the concentration of PCF-mpz a maximum at $X_{PCF\text{-}mpz}$ = 0.67 is observed, theorizing a 2:1 PCF-mpz:Fe^{III} ratio. Secondly, the linearity of the segments in the Job's plots also indicates the formation of stable complexes[114a]. Consequently, PB shows a stable formation than PB-mpz. The greater the number of cyanide bridges, the more stable is the complex.

Based on this result, the chemical formula for PB and PB-mpz are represented in **Equation 25** and **26**, respectively.

$$KFe[Fe(CN)_6] \quad (\mathbf{25})$$

$$KFe[Fe(CN)_5(mpz)]_2 \quad (\mathbf{26})$$

Considering these results, models for this complex were drawn (**Figure 36**). PB has a representation as its crystal[115], with a 1:1 HCF:Fe^{III} ratio. For comparison, a part of PB-mpz crystal was modulated in a face-centered cubic unit cell, as well (with a 2:1 PCF-mpz:Fe^{III} ratio).

Significant number of defects in the structure can be seen (**Figure 36b**), but some considerations need to be taken into account. One contribution is the relative *trans* influence occasioned by mpz. CN^- *trans* to ligand has a shorter lengths to $Fe_{(C)}$ due the stronger σ-donation and π-receptor abilities of this group[24, 27]. Then, when PB-mpz is formed, the stabilization of d orbitals, occasioned by the presence of $Fe_{(N)}$ weakens the Fe-mpz bond, facilitating ligand exchange (see section **4.3.2**). It was observed that the purple color of PB-mpz solution turns blue with time and a study about the PB-mpz solution stability needs to be performed.

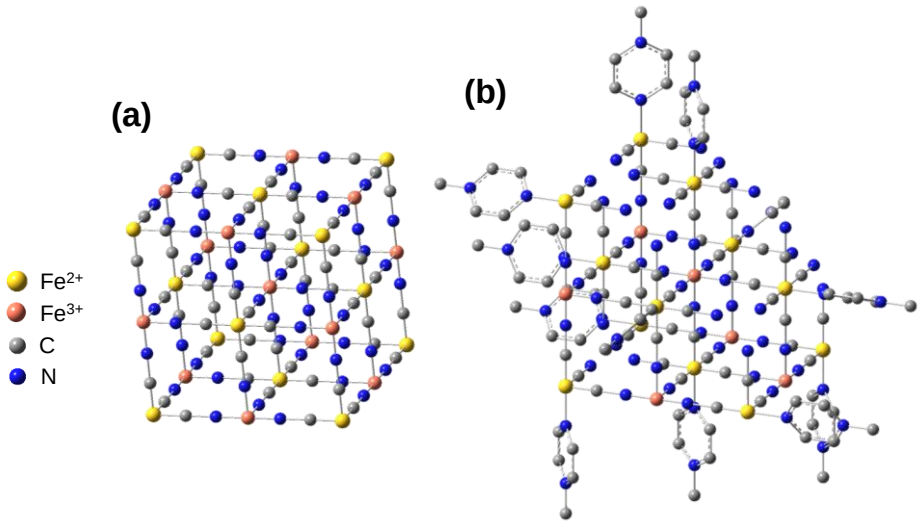

Figure 36. Proposed ferric cyanidoferrate(II) models. a) PB with 1:1 ratio. b) PB-mpz with 2:1 PCF-mpz ratio. Hydrogens are hidden for a better view of the structure.

According to the stoichiometries (**Equation 26**), some Fe^{III} needs to coordinate with solvent. **Figure 37** represents a plane of this proposed model and shows two Fe^{III} coordinated with different number of H_2O. Another interesting conclusion is about the volume occupied by mpz in this structure. If iron(II) of the center of **Figure 37** is considered, it is reasonable to think that

iron(III), bridged with it, cannot coordinate with other CN^- parallel to mpz. As a consequence, this site will be occupied by water, leaving some free space along the arrangement. The last point to be discussed is about the bond distances. As mentioned, the presence of mpz shortens the distance of *trans* CN^-, thus some geometry distortion occurs.

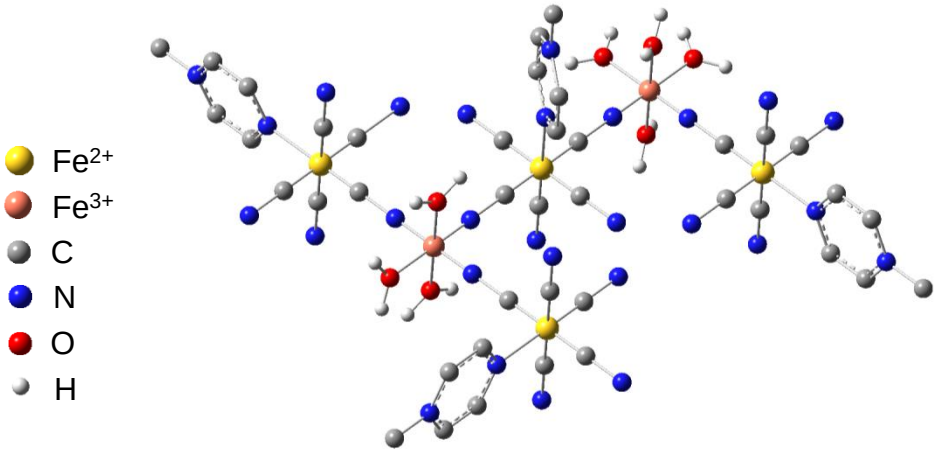

Figure 37. A plane of the proposed model. Hydrogens from mpz are hidden for a better view of the structure.

All these observations may contribute to formation of holes that can allow the presence of solvent, ions or small molecules. In an electrochemical point of view, defects in the structure can improve the performance of complex for analytical measurements[49]. These aspects and the presence of a positive charge (from mpz) need to be further evaluated.

Considering all the discussion above, PB-mpz appears to have an amorphous arrangement or a low crystallinity (not a face-centered cubic structure like PB).

4.3.6. X-ray Diffraction

X-ray diffraction (XRD) was used to compare the crystallinity of PB with PB-mpz. Thus, **Figure 38** shows XRD from this species. PB presented peaks at 17.49; 24.73; 35.44; 39.67; 43.73; 50.71; 54.24 and 57.41º, which correspond to (100), (110), (200), (210), (211), (300) and (310) planes, respectively. This

result is consistent with JCPDS (N 01-0239) standard, indicating a face-centered cubic structure for PB.

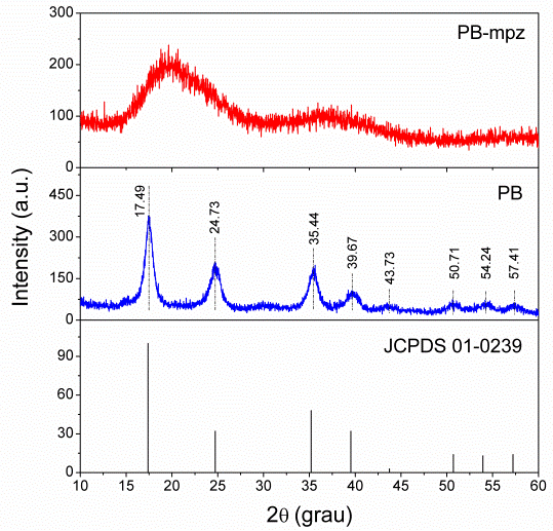

Figure 38. XRD from PB (plus standard) and PB-mpz

While PB has many peaks, PB-mpz shows two broad peaks. However, it is possible to see a relationship between the peaks of PB and the broad peaks of PB-mpz, meaning that the structures of both are similar. The difference is that the peaks broadness indicates a random atomic distribution, i.e., a short-range atomic distribution. Some evidences about the compound disorganization are mentioned in previous topics. This is in agreement with XRD data. It is possible to assume that the presence of mpz in the structure turns PB-mpz amorphous.

4.4. PB-mpz films

The chosen electrode modification method was the drop-casting due to reproducibility problem of PB-mpz electrodeposition. Firstly, it was tested the modification method employed by Pires[9] et al. (cited in the section **1.4.4**). However, the oxidation of PCF-mpz takes more time to occur and appeared to make mpz labile[6], hindering the reproduction of the modification. Moreover, the amount of deposited film was low. Then, the drop-casting method was chosen and, later, PB was synthesized directly on the electrode surface, layer-by-layer.

This method cannot guarantee the amount of deposited film, but allows a good response. Consequently, the analysis that depended on the current generated was compared via current density (j).

Other points that need to be analyzed are: the stability of PB-mpz in buffer solutions; the stability of PB-mpz films; the working potential uses to detect the analyte; and the detection of the analyte. These experiments are discussed in more details in the next sections.

4.4.1. The stability of PB-mpz in buffer and salt solutions

Similar experiment described in section **3.3.6** and discussed in section **4.2.5.2** was tried to PB-mpz. However, for all the pH values the electronic spectra showed the same behavior. **Figure 39** shows the electronic spectra of PB-mpz in aqueous and buffer (pH 3.0) solutions and PCF-mpz in aqueous solution.

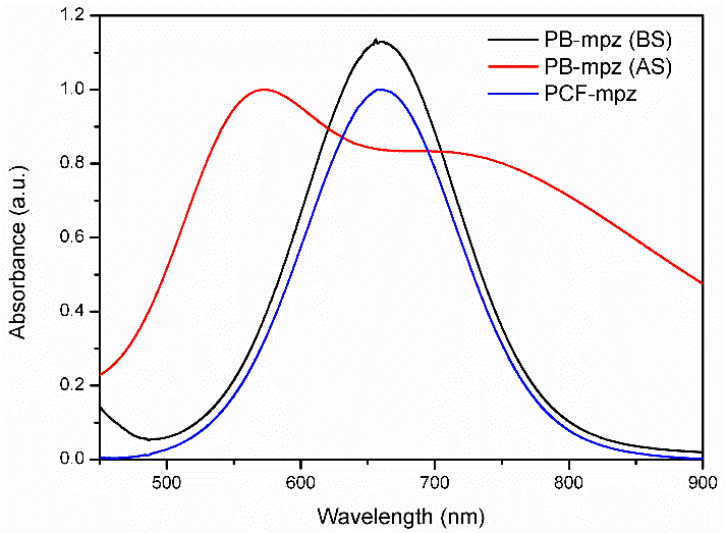

Figure 39. Electronic spectra of PB-mpz in aqueous (AS) and buffer (BS) solutions and PCF-mpz in aqueous solution.

These results suggest that there are species in the Britton-Robinson buffer that are able to break the Fe-CN-Fe bond, resulting in a characteristic spectrum of the complex, which presents transition of PCF-mpz (MLCT). This buffer contains orthoborate, acetate and phosphate ions. In order to analyze the

effect of these ions, electronic spectra of ferric chloride, PB and PB-mpz in presence of acetate, orthoborate and phosphate salts were collected. For comparison, spectra containing sulfate salt solutions were also collected (**Figure 40**).

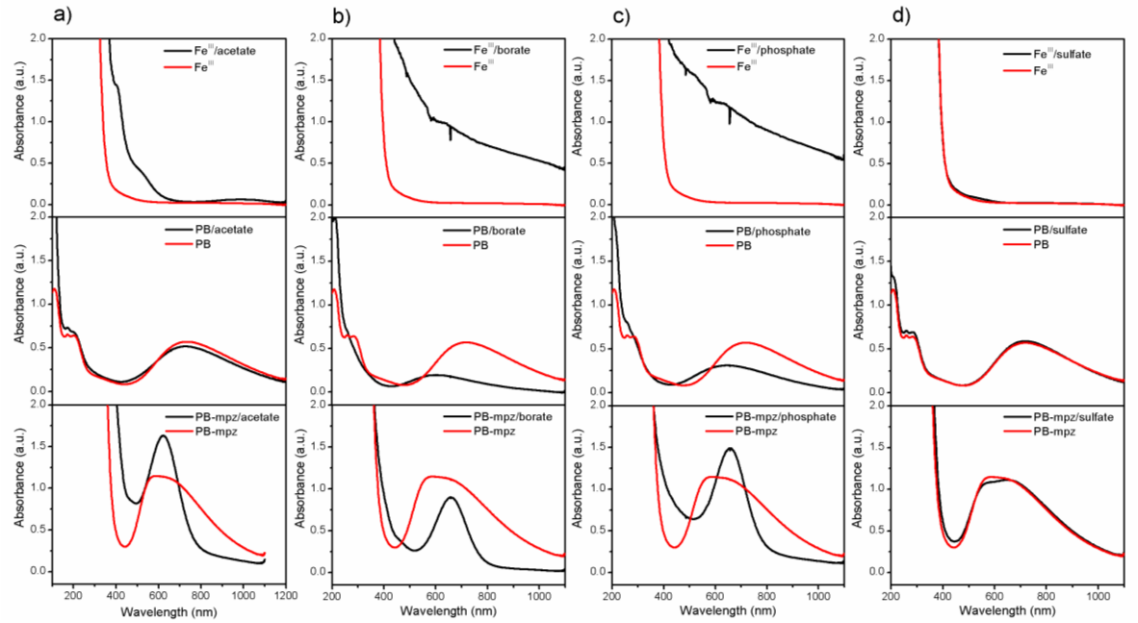

Figure 40. Electronic spectra of: (a) acetate; (b) borate; (c) phosphate and (d) sulfate ions as tests solutions with iron(III), PB and PB-mpz.

The changes in the spectrum indicate the formation of products. It is then possible to say if a reaction occurs. **Table 8** shows the summary of this conclusion:

Table 8. Salt ions reaction summary.

Salt ion	Fe^{III}	PB	PB-mpz
Acetate	Reacts[a]	Reacts Little	Reacts
Borate	Reacts[b]	Reacts	Reacts
Phosphate	Reacts[b]	Reacts	Reacts
Sulfate	-	-	-

[a] soluble product; [b] insoluble product.

Analyzing the data (**Figure 40** and **Table 8**), it is possible to conclude that the salt ions present in the buffer can react with iron(III) ions. Additionally,

in the presence of PB and PB-mpz, these salt ions are shown to be able to withdraw Fe^{3+}, breaking the cyanide bridge. Acetate ion was able to cause small alterations in PB spectrum, while in PB-mpz it changes drastic (**Figure 40a**). Acetate ions can coordinate to iron(III), but the complex formed is soluble, occasioning a lower number of breaks in PB structure. In PB-mpz the effect is faster, due to higher number of Fe^{III}-OH_2 bonds and disorganized chains. In addition, borate and phosphate ions, in the presence of both PB and PB-mpz, change their spectra drastically. These salt ions attract iron(III) ions, forming insoluble iron salts, shifting the background line (**Figure 40b** and **40c**). Moreover, the data showed that the sulfate ions do not react with iron(III) in these conditions (**Figure 40d**). Iron(III) sulfate is an ionic and soluble compound, consequently it does not interfere on the PB and PB-mpz structures.

Although PB solution differs from PB-based films, it is important to take these observations into account. In PB-based films prepared for electrochemical measurements, the solution contains KCl (as electrolyte support) and the redox processes can stabilize the compound, as seen in section **1.4.4**. Thus, the next topic describes the stability of PB-mpz films.

4.4.2. The stability of PB-mpz films

Due to anions problem discussed above, two buffer solutions were used to compare the stability of PB and PB-mpz films: HCl-KCl and Britton-Robinson (BR) buffer, both at pH 2.0. Then, the stability of the films was established by applying several cycles and evaluating the current peak of the redox processes of the immobilized species (**Figure 41**).

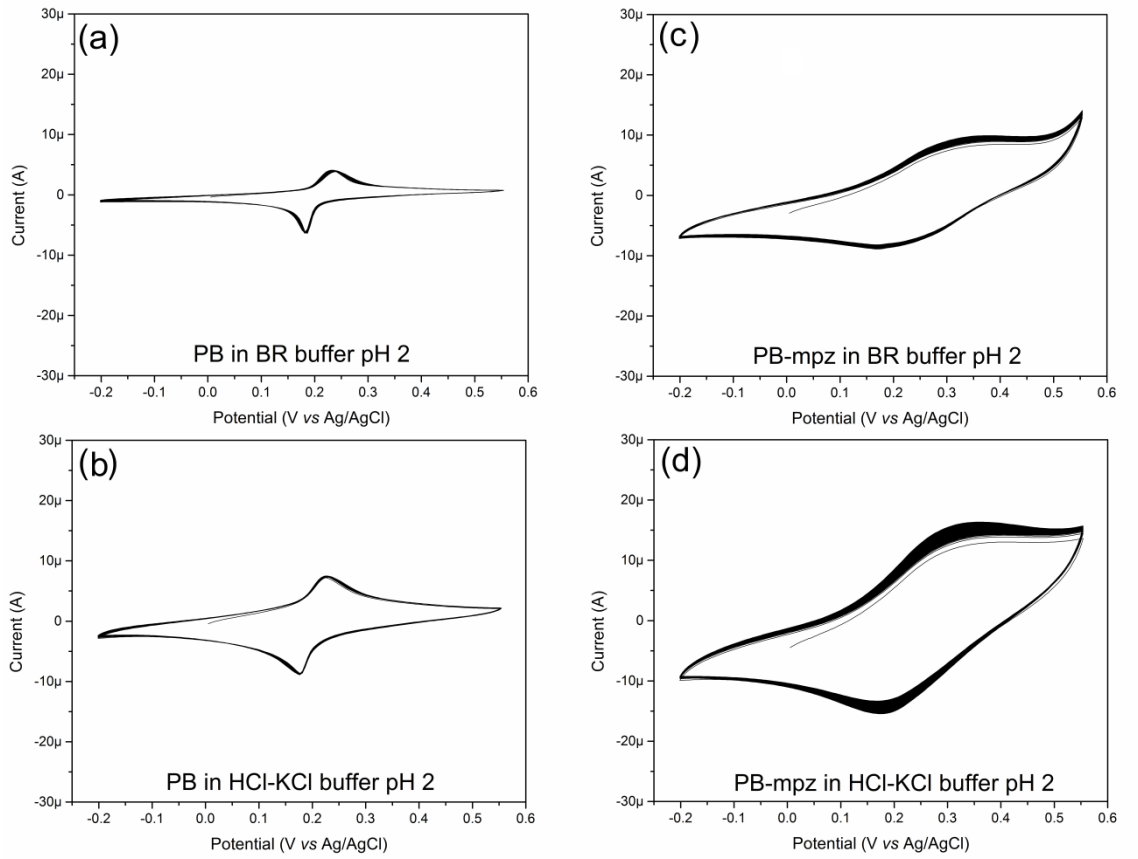

Figure 41. Stability of PB modified electrodes in (a) BR and (b) HCl-KCl buffer solutions; and PB-mpz modified electrodes in (c) BR and (d) HCl-KCl buffer solutions. Data collected with KCl 0.1 mol L^{-1} as support electrolyte, scan rate of 50 mV s^{-1} and pH 2.0.

Both PB and PB-mpz modified electrodes showed a good stability after consecutive cycles. In order to analyze the electrochemical response of PB and PB-mpz in buffer solutions, **Table 9** describes the potential and current peaks of the redox processes for the first and last cycles. After the deposition step the composition of the films are associated to the insoluble form. However, multiple cycles around the redox PB-PW processes turn the compounds to soluble forms, due to insertion of potassium ion on the structure[70]. The low pH provides H^+ that can also penetrate the defects of the structures[116], decreasing the charge density around the iron ions, increasing the oxidation potential of $Fe_{(N)}$ (see section **4.3.2**, for comparison). Additionally, the cycling step protects the $Fe_{(N)}$ from the anions, changing the oxidation state of this metal consecutively.

Table 9. Potential and current peaks at the first and last cycles of modified electrodes in buffer solutions.

		PB				**PB-mpz**			
		mV		μA		mV		μA	
Buffer	Cycle	E_{ap}	E_{cp}	i_{ap}	i_{cp}	E_{ap}	E_{cp}	i_{ap}	i_{cp}
BR	1st	0.23	0.19	4.04	-6.43	0.41	0.17	8.47	-8.33
	100th	0.24	0.18	3.85	-6.21	0.38	0.17	9.93	-8.91
HCl-KCl	1st	0.23	0.19	1.16	-1.61	0.30	0.18	7.40	-7.64
	100th	0.23	0.18	1.25	-1.81	0.32	0.18	8.56	-9.00

Based on this, after the 100th cycle, it is possible to see that PB increases the oxidation potential by ~0.02 mV in both BR and HCl-KCl buffers, while PB-mpz increases by ~0.11 and ~0.05 mV in BR and HCl-KCl buffer, respectively (compared with data obtained in aqueous solutions – section **4.3.2**). Consequently, the anions of BR buffer can be interfering in the oxidation potential of PB-mpz. Moreover, the final current peak is a bit lower only in the PB film in BR buffer. Then, due to the great variation in the E_{ap} of PB-mpz and the low film loss of PB in BR buffer, HCl-KCl buffer solutions was chosen to further work.

Furthermore, **Figure 41** shows a greater current peak for PB-mpz than PB, indicating a high amount of PB-mpz in the surface of the electrode. Thus, the electroactive areas of the modified electrodes were determined (**Equation 16**) before and after the cycles to compare them in function of the current density (**Table 10**).

Table 10. Electroactive area and current density of the electrodes, after and before 100 cycles, in the presence of HCl-KCl buffer (pH 2.0).

Electroactive area (cm^2)				
Clean	Initially		After the cycles	
4.45×10^{-2}	PB	PB-mpz	PB	PB-mpz
	4.32×10^{-2}	11.10×10^{-2}	4.33×10^{-2}	8.49×10^{-2}
	Current density ($\mu A/cm^2$)			
	10.45	171.30	14.72	197.69

These results show that the charge flow involved in PB-mpz film is greater than in PB film. This can be attributed to higher superface area and defects in the structure of the PB-mpz, when compared to PB solid, in agreement with the proposed by Job's method (section **4.3.5**). Moreover, the amount of immobilized species had no significant loss after the cycles.

4.4.3. The choice of the working potential

Most of the hydrogen peroxide sensors based on PB modifiec electrodes apply a working potential of 0 or -0.05 V *vs* Ag/AgCl[70]. To the improvement of H_2O_2 response, PB-based modified electrodes were used to analyze the best potential to reduce the analyte (**Figure 42**). With addition of hydrogen peroxide, PB shows slight decrease of cathodic current and a wave appears at negatives potential, with good linear response at -0.1 V *vs* Ag/AgCl. In contrast, PB-mpz modified electrode showed a significant variation at the potential that PB-mpz/PW-mpz process occurs (0.18 V *vs* Ag/AgCl). The structure defects can be directly influencing the interaction of electroactive molecule and PB-mpz film.

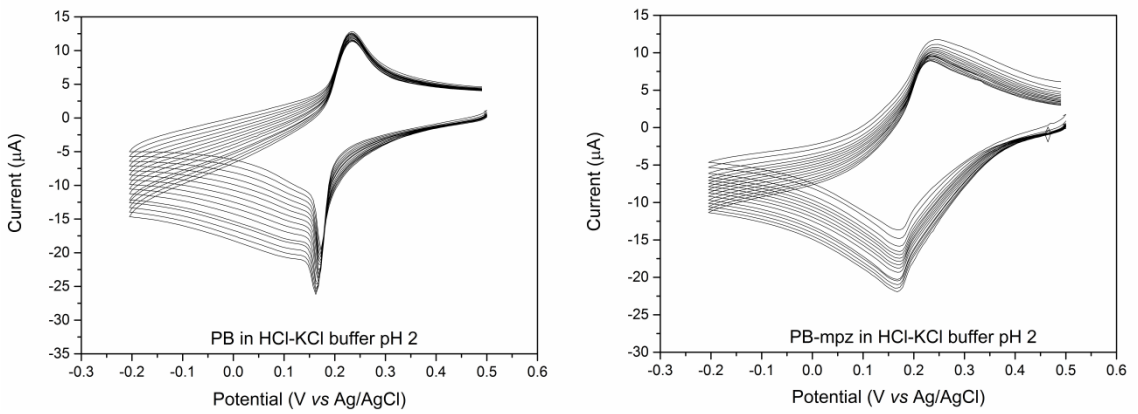

Figure 42. Electrochemical behavior of PB (left) and PB-mpz (right) modified electrode in the presence of different concentrations of H_2O_2 in HCl-KCl buffer solution (pH 2.0).

On the other hand, PB reduction potential shifts to lower values, being an indication of degradation of the film. Iron(II) formed on reduction process can rapidly react with H_2O_2, producing iron(III) hydroxide if the solution pH is high or not buffered. The new reduction process can be associated to HCF released from the PB layer during H_2O_2 reduction[117].

4.4.4. Electrochemical reduction of hydrogen peroxide

Through the voltammograms presented in **Figure 42**, the working potential window used in the chronoamperometric measurements was defined as -0.1 and 0.18 V *vs* Ag/AgCl for PB and PB-mpz films, respectively. **Figure 43** shows the chronoamperogram of the modified electrodes after addition of hydrogen peroxide solution.

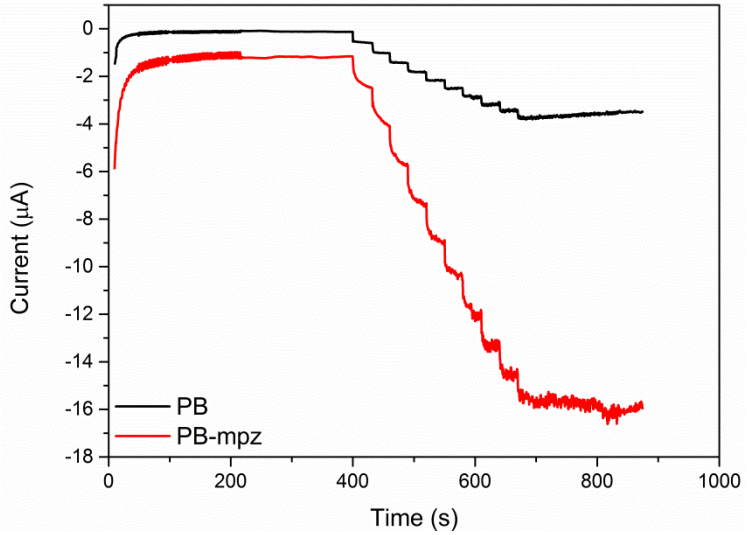

Figure 43. Chronoamperometric detection of hydrogen peroxide using the modified electrodes in KCl-HCl buffer (pH 2.0). Working potential: -0.1 and 0.18 V *vs* Ag/AgCl for PB and PB-mpz, respectively.

Increasing the total concentration of H_2O_2 on the solution leads to a lowering in the difference of the current intensity, occasioned by gradual decomposition of the films as observed in **Figure 42**. The film loss increased in BR buffer solution. However, the PB-based films showed good sensibility for H_2O_2, especially PB-mpz. The reduction of the analyte at the same reduction potential of iron increases the response. The analytical curves (**Figure 44**) were obtained from the chronoamperograms.

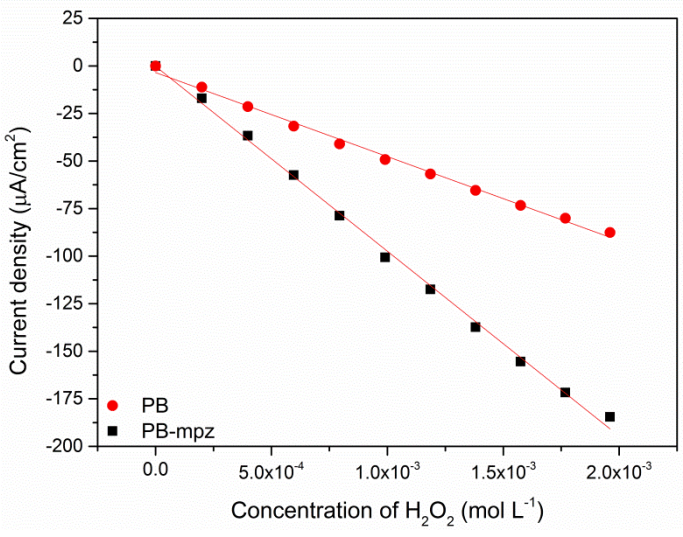

Figure 44. Analytical curves obtained from chronoamperometric detection of hydrogen peroxide using the modified electrodes in KCl-HCl buffer (pH 2.0).

The PB-based modified electrodes show a linear response to hydrogen peroxide reduction in the range of 0 to 2.5 mmol L^{-1}. The limit of detection was estimated to 7.39 x 10^{-5} and 1.11 x 10^{-4} mol L^{-1}, for PB and PB-mpz, respectively. This high value is due to the high concentration of stock solution (0.1 mol L^{-1}).

However, PB-mpz shows potential application for hydrogen peroxide detection. Various techniques are in agreement with the high quantity of defects in PB-mpz structure than in PB structure. The presence of mpz in this compound resulted in several properties that differentiate it from traditional Prussian blue.

5. FINAL CONSIDERATIONS

The mpz ligand and the pentacyanidoferrate(II) $[Fe(CN)_5(mpz)]^{2-}$ were synthesized and characterized for comparison with PB-mpz. Even though the spectroscopic properties of mpz are known, there is little information about its electrochemical behavior. Mpz• is formed by reducing mpz. This radical rapidly reacts, featuring an EC_i mechanism, allowing to calculate the rate constant of mpz• reaction (1.003 x 10^2 s^{-1}). However, in acidic medium mpz• reacts with H^+, forming a less reactive species, that allows a quasi-reversible process. Analogously, mpz coordination with PCF turns mpz• less reactive, increasing the oxidation potential of iron and forming a stable compound with a dissociation rate constant of 3.78 x 10^{-4} s^{-1}. Studies at various pH values have shown that PCF-mpz is more stable at pH < 7.0.

PB-mpz has been characterized and the presence of mpz was evaluated using spectroscopic techniques, cyclic voltammetry, spectroelectrochemistry, Job's method and X-ray diffraction. Formation of PB-mpz leads to a change in the electronic structures, compared to PB. Cyclic voltammetry has shown that the mpz ligand is on the PB structure. Spectroelectrochemistry confirms IT band and a dislocation of the MLCT, in reduction potentials. Infrared spectrum showed characteristics of PB and mpz, in agreement with other experiments. Job's method gives a proportion of 1:1 HCF:Fe^{III} and 2:1 PCF-mpz:Fe^{III}, indicating low crystallinity for the second. XRD confirms that PB-mpz is amorphous. Study at various pH values has shown that PB-mpz has broken its

structure. Tests with salts present in Britton-Robinson buffer have shown that they react with Fe^{3+} ions of PB-mpz.

Additionally, PB-based films were evaluated in BR and HCl-KCl buffers. The HCl-KCl obtained a better electrochemical response. PB-mpz film showed better sensitivity to H_2O_2 than PB film. The reduction potential of H_2O_2 occurs at the same potential as PW-mpz/PB-mpz. The limits of detection were 7.39×10^{-5} and 1.11×10^{-4} mol L^{-1}, for PB and PB-mpz, respectively.

Limitations on the use of PB-based modified electrodes, such as low stability in higher pH and the film loss in the presence of hydrogen peroxide needs to be minimized. The next steps include interfering test in the determination of H_2O_2 (such as ascorbic and uric acids and dopamine) and tests with different analytes, such as cysteine. From these results, it is intended to determine the viability of using this material in portable biosensors (point of care).

6. REFERENCES

[1] D. H. Macartney, *Reviews in Inorganic Chemistry* **1988**, *9*, 101-152.

[2] L. M. Baraldo, P. Forlano, A. R. Parise, L. D. Slep, J. A. Olabe, *Coordination Chemistry Reviews* **2001**, *219*, 881-921.

[3] aH. E. Toma, J. M. Malin, *Inorganic Chemistry* **1973**, *12*, 1039-1045; bH. E. Toma, J. M. Malin, *Inorganic Chemistry* **1973**, *12*, 2080-2083.

[4] S. H. Toma, J. A. Bonacin, K. Araki, H. E. Toma, *European journal of inorganic chemistry* **2007**, *2007*, 3356-3364.

[5] C. X. Zhang, S. J. Lippard, *Current opinion in chemical biology* **2003**, *7*, 481-489.

[6] H. E. Toma, C. Creutz, *Inorganic Chemistry* **1977**, *16*, 545-550.

[7] H. E. Toma, A. A. Batista, *Journal of inorganic biochemistry* **1984**, *20*, 53-59.

[8] F. M. Matsumoto, M. L. Temperini, H. E. Toma, *Electrochimica acta* **1994**, *39*, 385-391.

[9] B. Morandi Pires, S. A. Venturinelli Jannuzzi, A. L. Barboza Formiga, J. Alves Bonacin, *European Journal of Inorganic Chemistry* **2014**, *2014*, 5812-N5819.

[10] aM. B. Robin, *Inorganic Chemistry* **1962**, *1*, 337-342; bK. Itaya, I. Uchida, V. D. Neff, *Accounts of Chemical Research* **1986**, *19*, 162-168.

[11] A. A. Karyakin, *Electroanalysis* **2001**, *13*, 813-819.

[12] B. Mayoh, P. Day, *Journal of the Chemical Society, Dalton Transactions* **1976**, 1483-1486.

[13] M. Hirscher, B. Panella, B. Schmitz, *Microporous and mesoporous materials* **2010**, *129*, 335-339.

[14] D. Santos, P. Saturnino, R. Lobo, C. Sequeira, *Journal of Power Sources* **2012**, *208*, 131-137.

[15] G. Fu, X. Yue, Z. Dai, *Biosensors and Bioelectronics* **2011**, *26*, 3973-3976.

[16] E. Waldhör, W. Kaim, J. A. Olabe, L. D. Slep, J. Fiedler, *Inorganic chemistry* **1997**, *36*, 2969-2974.

[17] H. E. Toma, *Canadian Journal of Chemistry* **1979**, *57*, 2079-2084.

[18] S. Alshehri, J. Burgess, R. van Eldik, C. D. Hubbard, *Inorganica chimica acta* **1995**, *240*, 305-311.

[19] G. t. Cheeseman, E. Werstiuk, *Advances in heterocyclic chemistry* **1972**, *14*, 99-209.

[20] A. Albert, A. Katritzky, *by AR Katritzky, Academic Press, New York* **1963**, 1.

[21] A. S.-c. Chia, R. Trimble Jr, *The Journal of Physical Chemistry* **1961**, *65*, 863-866.

[22] C. T. Bahner, L. L. Norton, *Journal of the American Chemical Society* **1950**, *72*, 2881-2882.

[23] C. Yang, M.-S. Wang, Z.-N. Xu, F. Chen, G.-N. Liu, G. Xu, G.-C. Guo, J.-S. Huang, *Inorganic Chemistry Communications* **2010**, *13*, 326-329.

[24] A. L. B. Formiga, S. Vancoillie, K. Pierloot, *Inorganic chemistry* **2013**, *52*, 10653-10663.

[25] J. E. Figard, J. V. Paukstelis, E. F. Byrne, J. D. Petersen, *Journal of the American Chemical Society* **1977**, *99*, 8417-8425.

[26] D. A. Estrin, O. Y. Hamra, L. Paglieri, L. D. Slep, J. A. Olabe, *Inorganic chemistry* **1996**, *35*, 6832-6837.

[27] B. J. Coe, S. P. Foxon, E. C. Harper, J. Raftery, R. Shaw, C. A. Swanson, I. Asselberghs, K. Clays, B. S. Brunschwig, A. G. Fitch, *Inorganic chemistry* **2009**, *48*, 1370-1379.

[28] H. Börzel, P. Comba, K. S. Hagen, Y. D. Lampeka, A. Lienke, G. Linti, M. Merz, H. Pritzkow, L. V. Tsymbal, *Inorganica chimica acta* **2002**, *337*, 407-419.

[29] T. Damhus, R. M. Hartshorn, A. T. Hutton, *Nomenclature of inorganic chemistry: IUPAC recommendations 2005*, Royal Society of Chemistry, **2005**.

[30] aJ. Kyd, *The London, Edinburgh, and Dublin Philosophical Magazine and Journal of Science* **1850**, *37*, 289-291; bW. Gordy, D. Williams, *The Journal of Chemical Physics* **1935**, *3*, 664-667.

[31] E. Fluck, W. Kerler, W. Neuwirth, *Angewandte Chemie International Edition in English* **1963**, *2*, 277-287.

[32] D. Kenney, T. Flynn, J. Gallini, *Journal of Inorganic and Nuclear Chemistry* **1961**, *20*, 75-81.

[33] H. E. Toma, J. M. Malin, *Inorganic Chemistry* **1974**, *13*, 1772-1774.

[34] G. Davies, A. R. Garafalo, *Inorganic Chemistry* **1980**, *19*, 3543-3544.

[35] J. E. Figard, J. D. Petersen, *Inorganic Chemistry* **1978**, *17*, 1059-1063.

[36] K. J. Moore, L. Lee, G. A. Mabbott, J. D. Petersen, *Inorganic Chemistry* **1983**, *22*, 1108-1112.

[37] A. P. Szecsy, A. Haim, *Journal of the American Chemical Society* **1981**, *103*, 1679-1683.

[38] S. Kawanishi, W. Caughey, *Journal of Biological Chemistry* **1985**, *260*, 4622-4631.

[39] F. Felix, A. Ludi, *Inorganic Chemistry* **1978**, *17*, 1782-1784.

[40] N. Ghasdian, Y. Liu, R. McHale, J. He, Y. Miao, X. Wang, *Journal of Inorganic and Organometallic Polymers and Materials* **2013**, *23*, 111-118.

[41] H. E. Toma, Universidade de São Paulo **1979**.

[42] J. Brown, *Philosophical Transactions* **1724**, *33*, 17-24.

[43] A. Kraft, *Bulletin for the History of Chemistry* **2008**, *33*, 61-67.

[44] L. Coleby, *Annals of Science* **1939**, *4*, 206-211.

[45] J. Keggin, F. Miles, *Nature* **1936**, *137*, 577-578.

[46] H. Buser, D. Schwarzenbach, W. Petter, A. Ludi, *Inorganic Chemistry* **1977**, *16*, 2704-2710.

[47] P. J. Faustino, Y. Yang, J. J. Progar, C. R. Brownell, N. Sadrieh, J. C. May, E. Leutzinger, D. A. Place, E. P. Duffy, F. Houn, *Journal of pharmaceutical and biomedical analysis* **2008**, *47*, 114-125.

[48] V. D. Neff, *Journal of the Electrochemical Society* **1978**, *125*, 886-887.

[49] Q. Shen, J. Jiang, M. Fan, S. Liu, L. Wang, Q. Fan, W. Huang, *Journal of Electroanalytical Chemistry* **2014**, *712*, 132-138.

[50] K. Itaya, N. Shoji, I. Uchida, *Journal of the American Chemical Society* **1984**, *106*, 3423-3429.

[51] M. Jayalakshmi, F. Scholz, *Journal of power sources* **2000**, *87*, 212-217.

[52] Y. Jiang, S. Yu, B. Wang, Y. Li, W. Sun, Y. Lu, M. Yan, B. Song, S. Dou, *Advanced Functional Materials* **2016**.

[53] D. Davidson, *J. Chem. Educ* **1937**, *14*, 238.

[54] S. Pintado, S. Goberna-Ferrón, E. C. Escudero-Adán, J. R. n. Galán-Mascarós, *Journal of the American Chemical Society* **2013**, *135*, 13270-13273.

[55] S. Mitra, V. Sharma, N. Thakur, S. Yusuf, F. Juranyi, R. Mukhopadhyay, in *EPJ Web of Conferences, Vol. 83*, EDP Sciences, **2015**, p. 02012.

[56] aA. Ludi, H. U. Güdel, in *Inorganic Chemistry*, Springer, **1973**, pp. 1-21; bF. Herren, P. Fischer, A. Ludi, W. Hälg, *Inorganic Chemistry* **1980**, *19*, 956-959.

[57] L. D. Hansen, W. M. Litchman, G. H. Daub, *J. Chem. Educ* **1969**, *46*, 46.

[58] P. W. Ayers, *Faraday Discussions* **2007**, *135*, 161-190.

[59] M. Ware, *J. Chem. Educ* **2008**, *85*, 612.

[60] P. S. Braterman, *Reactions of coordinated ligands, Vol. 2*, Springer Science & Business Media, **2012**.

[61] X. Roy, M. J. MacLachlan, *Chemistry–A European Journal* **2009**, *15*, 6552-6559.

[62] aJ. Agrisuelas, J. García-Jareño, C. Moreno-Guerrero, A. Roig, F. Vicente, *Electrochimica Acta* **2013**, *113*, 825-833; bP. R. Somani, S. Radhakrishnan, *Materials chemistry and physics* **2003**, *77*, 117-133.

[63] aP. Somani, S. Radhakrishnan, *Chemical physics letters* **1998**, *292*, 218-222; bR. J. Mortimer, D. R. Rosseinsky, *Journal of the Chemical Society, Dalton Transactions* **1984**, 2059-2062.

[64] A. Roig, J. Navarro, J. Garcia, F. Vicente, *Electrochimica acta* **1994**, *39*, 437-442.

[65] H. D. Abruña, *Coordination Chemistry Reviews* **1988**, *86*, 135-189.

[66] C. Lundgren, R. W. Murray, *Inorganic Chemistry* **1988**, *27*, 933-939.

[67] T. Ozeki, I. Watanbe, S. Ikeda, *Journal of electroanalytical chemistry and interfacial electrochemistry* **1987**, *236*, 209-218.

[68] K. Itaya, H. Akahoshi, S. Toshima, *Journal of the Electrochemical Society* **1982**, *129*, 1498-1500.

[69] H. Gomathi, G. P. Rao, *Journal of Applied Electrochemistry* **1990**, *20*, 454-456.

[70] F. Ricci, G. Palleschi, *Biosensors and Bioelectronics* **2005**, *21*, 389-407.

[71] M. Vidotti, S. I. C. de Torresi, *Electrochimica Acta* **2009**, *54*, 2800-2804.

[72] T.-C. Liao, W.-H. Chen, H.-Y. Liao, L.-C. Chen, *Solar Energy Materials and Solar Cells* **2016**, *145*, 26-34.

[73] Q. Zhang, L. Zhang, J. Li, *Electrochimica Acta* **2008**, *53*, 3050-3055.

[74] I. L. de Mattos, L. V. Lukachova, L. Gorton, T. Laurell, A. A. Karyakin, *Talanta* **2001**, *54*, 963-974.

[75] P. Pandey, D. Panday, *Electrochimica Acta* **2016**, *190*, 758-765.

[76] R. Koncki, *Critical Reviews in Analytical Chemistry* **2002**, *32*, 79-96.

[77] E. A. Veal, A. M. Day, B. A. Morgan, *Molecular Cell*, *26*, 1-14.

[78] P. L. dos Santos, **2015**.

[79] I. L. d. Mattos, K. A. Shiraishi, A. D. Braz, J. R. Fernandes, *Química Nova* **2003**, *26*, 373-380.

[80] Y. T. Didenko, S. Pugach, *The Journal of Physical Chemistry* **1994**, *98*, 9742-9749.

[81] C. Matsubara, N. Kawamoto, K. Takamura, *Analyst* **1992**, *117*, 1781-1784.

[82] A. Sakuragawa, T. Taniai, T. Okutani, *Analytica chimica acta* **1998**, *374*, 191-200.

[83] M. Navas, A. Jimenez, G. Galan, *Atmospheric environment* **1999**, *33*, 2279-2283.

[84] E. W. Kellogg, I. Fridovich, *Journal of biological chemistry* **1975**, *250*, 8812-8817.

[85] F. Haber, J. Weiss, in *Proceedings of the Royal Society of London A: Mathematical, Physical and Engineering Sciences, Vol. 147*, The Royal Society, **1934**, pp. 332-351.

[86] J. J. Lingane, P. J. Lingane, *Journal of Electroanalytical Chemistry (1959)* **1963**, *5*, 411-419.

[87] R. S. Rocha, R. M. Reis, A. A. G. F. Beati, M. R. V. Lanza, M. D. P. T. Sotomayor, R. Bertazzoli, *Química Nova* **2012**, *35*, 1961-1966.

[88] M. Vazquez, S. De Sanchez, E. Calvo, D. Schiffrin, *Journal of Electroanalytical Chemistry* **1994**, *374*, 179-187.

[89] A. A. Karyakin, O. V. Gitelmacher, E. E. Karyakina, *Analytical Letters* **1994**, *27*, 2861-2869.

[90] B. Kong, C. Selomulya, G. Zheng, D. Zhao, *Chemical Society Reviews* **2015**, *44*, 7997-8018.

[91] B. Kong, J. Tang, Z. Wu, C. Selomulya, H. Wang, J. Wei, Y. Wang, G. Zheng, D. Zhao, *NPG Asia Materials* **2014**, *6*, e117.

[92] L. Samain, F. Grandjean, G. J. Long, P. Martinetto, P. Bordet, D. Strivay, *The Journal of Physical Chemistry C* **2013**, *117*, 9693-9712.

[93] H. T. S. Britton, R. A. Robinson, *Journal of the Chemical Society (Resumed)* **1931**, 1456-1462.

[94] J. M. Malin, C. F. Schmidt, H. E. Toma, *Inorganic Chemistry* **1975**, *14*, 2924-2928.

[95] M. J. Blandamer, M. F. Fox, *Chemical Reviews* **1970**, *70*, 59-+.

[96] M. Pal, S. Bagchi, *Journal of the Chemical Society-Faraday Transactions I* **1985**, *81*, 2323-2331.

[97] aR. Foglizzo, A. Novak, *Applied Spectroscopy* **1970**, *24*, 601-+; bK. B. Hewett, M. H. Shen, C. L. Brummel, L. A. Philips, *Journal of Chemical Physics* **1994**, *100*, 4077-4086.

[98] S. A. V. Jannuzzi, B. Martins, M. I. Felisberti, A. L. B. Formiga, *Journal of Physical Chemistry B* **2012**, *116*, 14933-14942.

[99] C. Brett, M. O. Brett, A. M. C. M. Brett, A. M. O. Brett, *Electrochemistry: principles, methods, and applications*, **1993**.

[100] R. Iwamoto, *Analytical Chemistry* **1959**, *31*, 955-955.

[101] M. Castilho, L. E. Almeida, M. Tabak, L. H. Mazo, *Journal of the Brazilian Chemical Society* **2000**, *11*, 148-153.

[102] R. S. Nicholson, I. Shain, *Analytical Chemistry* **1964**, *36*, 706-723.

[103] J. Y. Kim, C. Lee, J. W. Park, *Journal of Electroanalytical Chemistry* **2001**, *504*, 104-110.

[104] D. R. Eaton, J. M. Watkins, R. J. Buist, *Journal of the American Chemical Society* **1985**, *107*, 5604-5609.

[105] J. W. Park, Y. Kim, C. Lee, *Bulletin of the Korean Chemical Society* **1994**, *15*, 896-900.

[106] H. Toma, Blucher: São Paulo, **2013**.

[107] K. R. Dunbar, R. A. Heintz, *Progress in Inorganic Chemistry, Vol 45* **1997**, *45*, 283-391.

[108] aD. T. Fagan, I. F. Hu, T. Kuwana, *Analytical chemistry* **1985**, *57*, 2759-2763; bP. H. Chen, M. A. Fryling, R. L. Mccreery, *Analytical chemistry* **1995**, *67*, 3115-3122.

[109] S. Konopka, B. McDuffie, *Analytical Chemistry* **1970**, *42*, 1741-1746.

[110] W. N. Perera, G. Hefter, *Inorganic chemistry* **2003**, *42*, 5917-5923.

[111] H. E. Toma, J. M. Malin, E. Giesbrecht, *Inorganic Chemistry* **1973**, *12*, 2084-2089.

[112] C. C. Corrêa, S. A. V. Jannuzzi, M. Santhiago, R. A. Timm, A. L. B. Formiga, L. T. Kubota, *Electrochimica Acta* **2013**, *113*, 332-339.

[113] P. J. Kulesza, M. A. Malik, A. Denca, J. Strojek, *Analytical chemistry* **1996**, *68*, 2442-2446.

[114] aZ. D. Hill, P. Maccarthy, *Journal of Chemical Education* **1986**, *63*, 162-167; bF. Woldbye, *Acta Chemica Scandinavica* **1955**, *9*, 299-309.

[115] H. J. Buser, A. Ludi, *Journal of the Chemical Society-Chemical Communications* **1972**, 1299-&.

[116] V. Plichon, S. Besbes, *Journal of electroanalytical chemistry and interfacial electrochemistry* **1990**, *284*, 141-153.

[117] J.-M. Noël, J. Médard, C. Combellas, F. Kanoufi, *ChemElectroChem* **2016**.